ADVANCED HEALTHCARE MATERIALS
www.advhealthmat.de

PEDOT:PSS-Based Bioelectronic Devices for Recording and Modulation of Electrophysiological and Biochemical Cell Signals

*Yuanying Liang, Andreas Offenhäusser, Sven Ingebrandt, and Dirk Mayer**

To understand the physiology and pathology of electrogenic cells and the corresponding tissue in their full complexity, the quantitative investigation of the transmission of ions as well as the release of chemical signals is important. Organic (semi-) conducting materials and in particular organic electrochemical transistor are gaining in importance for the investigation of electrophysiological and recently biochemical signals due to their synthetic nature and thus chemical diversity and modifiability, their biocompatible and compliant properties, as well as their mixed electronic and ionic conductivity featuring ion-to-electron conversion. Here, the aim is to summarize recent progress on the development of bioelectronic devices utilizing polymer polyethylenedioxythiophene: poly(styrene sulfonate) (PEDOT:PSS) to interface electronics and biological matter including microelectrode arrays, neural cuff electrodes, organic electrochemical transistors, PEDOT:PSS-based biosensors, and organic electronic ion pumps. Finally, progress in the material development is summarized for the improvement of polymer conductivity, stretchability, higher transistor transconductance, or to extend their field of application such as cation sensing or metabolite recognition. This survey of recent trends in PEDOT:PSS electrophysiological sensors highlights the potential of this multifunctional material to revolve current technology and to enable long-lasting, multichannel polymer probes for simultaneous recordings of electrophysiological and biochemical signals from electrogenic cells.

1. Introduction

Studying the connectivity and function of neurons in the brain is essential to decode the full complexity of information processing in central nervous systems. Advancements in related investigation methods (optogenetics,[1] neuroimaging,[2] and bioelectronics[3]) have been made to identify the type of involved neurons, to decipher the functions of specific regions in brain, and to untangle their wiring. Electrophysiological recordings provide quantitative data spanning multiple temporal and spatial scales, including the spiking activity of single neurons, network oscillations of small cell populations, and subthreshold activity during different brain states, thus facilitating a more encompassing understanding of brain activity.[4] The underlying electrophysiological mechanisms for the transmission of signals between electrogenic cells within nervous system or in muscular tissue are typically mediated by spatiotemporal variations of ionic concentrations, which are modulated by biomolecules.[5,6] Recording the chemical/physiological signals is thus of great importance to understand the activity of individual neurons and network functions as well as for the point-of-care disease diagnostics. Currently available methodologies for electrophysiological recoding of neural activities can be classified according to their scale:[7] a) Microscale intracellular recording and stimulation:[8,9] These techniques enable the recording of electrical signals of individual neurons and subthreshold synaptic activity by measuring currents of individual cells and even single ion channels via sharp (nanoneedle[8]) or patch electrodes.[10] This methodology exhibits excellent coupling between electrode and cell with high signal transmission coefficients, thus proving accurate readout of endogenous cell activity, subthreshold excitatory, and inhibitory synaptic inputs as well as resulting suprathreshold electrophysiological activity of neurons.[11] However, lacking scalability and the invasiveness of these membrane penetrating electrodes impairs their usage for long-term recordings.[11] b) Micro- and mesoscale extracellular recording and simulation: These measurements can be performed by numerous device platforms, including substrate-integrated microelectrode arrays (MEAs), electrolyte-gated field-effect transistors (FETs), and the in recent years emerging organic electrochemical

Dr. Y. Liang
Institute of Polymer Optoelectronic Materials and Devices
State Key Laboratory of Luminescent Materials and Devices
South China University of Technology
Guangzhou, Guangdong 510640, China
Prof. A. Offenhäusser, Dr. D. Mayer
Institute of Biological Information Processing
Bioelectronics IBI-3
Forschungszentrum Jülich Jülich 52425, Germany
E-mail: dirk.mayer@fz-juelich.de
Prof. S. Ingebrandt
Faculty of Electrical Engineering and Information Technology
Institute of Materials in Electrical Engineering 1
RWTH Aachen University
Aachen 52074, Germany

The ORCID identification number(s) for the author(s) of this article can be found under https://doi.org/10.1002/adhm.202100061

DOI: 10.1002/adhm.202100061

transistors (OECTs). Unlike the sharp and patch-clamp electrodes, the noninvasive extracellular techniques enable the simultaneous recording and stimulation of electrogenic cells over long time periods without mechanically damaging the cell membrane.[12,13,14] c) Macroscale measurement of wide areas brain's activities:[15] This method can be used to examine the functional connectivity of different regions in the brain, but with a lower spatial resolution. Accordingly, micro- and mesoscale extracellular recording sensors possess the greatest potential to facilitate simultaneous, multisite, long-term, and multiscale in vitro and in vivo recording from large populations of neurons.[16,17]

The main underlying challenge of extracellular recording of electrophysiological signals is the transduction of the modulation of ion concentrations at the interface between electrogenic cells and the receiving electronic devices to assure high signal-to-noise ratios. The coupling efficiency depends strongly on the seal resistance R_{seal} and the input impedance of the sensing device. The seal resistance R_{seal} is defined by the cleft formed between the cellular membrane and the device surface, which can be modulated by protruding nanostructures or nanocavities and it strongly depends on the cell adhesion.[11] Therefore, a high biocompatibility and a surface composition that facilitates a strong cell attachment is crucial for sensitive signal transduction. Especially interfacial materials of neuroelectronic hybrid systems that feature both, ion and electron conduction as well as a direct conversion between both conducting types, while enabling a low liquid-solid interface impedance, offer outstanding properties for the development of high-performance bioelectronic devices.[18]

The tremendous technological progress in microelectronic fabrication have fostered the development of bioelectronic devices based on solid-state materials including metals (Au, Pt) and semiconductors (silicone, compound semiconductors).[19,20] Recently, organic conjugated polymers have emerged as promising class of materials to engineer bioelectronic interfaces that are less invasive to biological matter. Unlike the conventional inorganic materials-based devices, whose operations are only dependent on the transport of electrons and holes, the organic semiconductor-based devices uniquely employ both ions and electrons as charge carriers and permit thus a direct signal transduction. Furthermore, their flexible and compliant mechanical properties[21] can alleviate the immune response of tissue caused by in vivo bioelectronic probes to a certain extend. Among these organic materials, the p-type conducting polymer polyethylenedioxythiophene and its doping poly(styrene sulfonate) (PEDOT:PSS) is the most widely utilized interfacial material for modern bioelectronics. Quite often it is described as the new golden standard for neuroelectronic interfaces. The success of PEDOT:PSS in this field is based on its combined electronic and ionic conductivity, commercial availability, flexibility, and biocompatibility. Furthermore, optical transparency of PEDOT:PSS in thin films permits simultaneous optical and electronic transduction in a single experiment.[22,23] Considering these merits, PEDOT:PSS electronics has been broadly employed for various bioelectronic device types, such as electrode coating, as electrode material, as channel material in OECTs or as ion conducting transport matrix in electrophoretic pumps. In this review article, we summarize recent progress on various PEDOT:PSS devices utilized to connect electronics with electrogenic cells with the aim to study the fundamental principles of signal transmission, the connectivity, and function of the corresponding tissue as well as engineering approaches to manipulate cellular activity by electrical and chemical stimuli (**Figure 1**).

2. Electrophysiological Sensors for Cell Recordings and Stimulation

Cells, as the smallest living entity of the human body, can have the capability to receive and transmit electrical signals mainly by utilizing ions and biomolecules regulating these processes. For electronically excitable cells, the cellular membrane can be described by the Hodgkin–Huxley model. Here the cytosol is separated from the extracellular environment by the capacitive lipid bilayer (**Figure 2**a). The cellular membrane is furthermore equipped with resistive, transmembrane ion-selective channels and pumps, which are capable of transferring different kinds of ions across the membrane (Figure 2b). At the resting state, the transmembrane potential of excitable cells has a negative value (neurons ≈ −75 mV) mainly caused by the imbalanced ion dispersion of excessive extracellular sodium (Na^+) and intracellular potassium (K^+) ions as well as the different permeability of the cellular membrane to these ions. Once an electrical input is applied either from a natural source such as a neighboring cell[34] or an external electrode (such as a patch-clamp pipette[35]), an alteration of the transmembrane potential occurs. Voltage-gated Na^+ channels open, when the transmembrane potential exceeds a certain threshold (≈−50 mV), enabling the rapid influx of Na^+ ions into the cell, which is accompanied with a depolarization of the cell. Correspondingly, the membrane potential increases significantly to roughly 35 mV in a short time (>2 ms),[36] followed by an efflux of K^+ ions to the extracellular environment. A repolarization of the membrane potential to the resting potential occurs afterward. The influx and efflux of ions result in the formation of local ionic currents and action potentials across cell membrane. Apart from the transportation of ions, the transmission of electrophysiological signals is governed on short and long-term by chemical signals mediated by the release of neurotransmitters (such as dopamine, acetylcholine, etc.) to the synapse.[37] The communication between neurons occurs through a special apposition of membranes and intermembrane machineries called synapse, which bridges the axon of one neuron (presynaptic terminal) and the dendrite of the other one (postsynaptic terminal) (Figure 2b). The chemical transmission across the synaptic cleft (width around 200–400 Å[38–40]) is primarily unidirectional in the mammalian brain. Close to the presynaptic terminal, there is an accumulation of vesicles filled with neurotransmitters, which are directly associated with specific neurological functions or, if misbalanced, with neurological diseases.[41] The release of these chemical transmitter-containing vesicles to the synaptic cleft is initiated by firing an action potential down to the presynaptic terminal. The chemical substances then diffuse to the receptor sites on the postsynaptic membrane, which changes the permeability of Na^+, thus inducing an alteration of the postsynaptic potential. Different from the action potential, which has a total amplitude of around 100 mV and a duration of 1–2 ms, the postsynaptic potential is in the range of a few milliseconds to tens of seconds

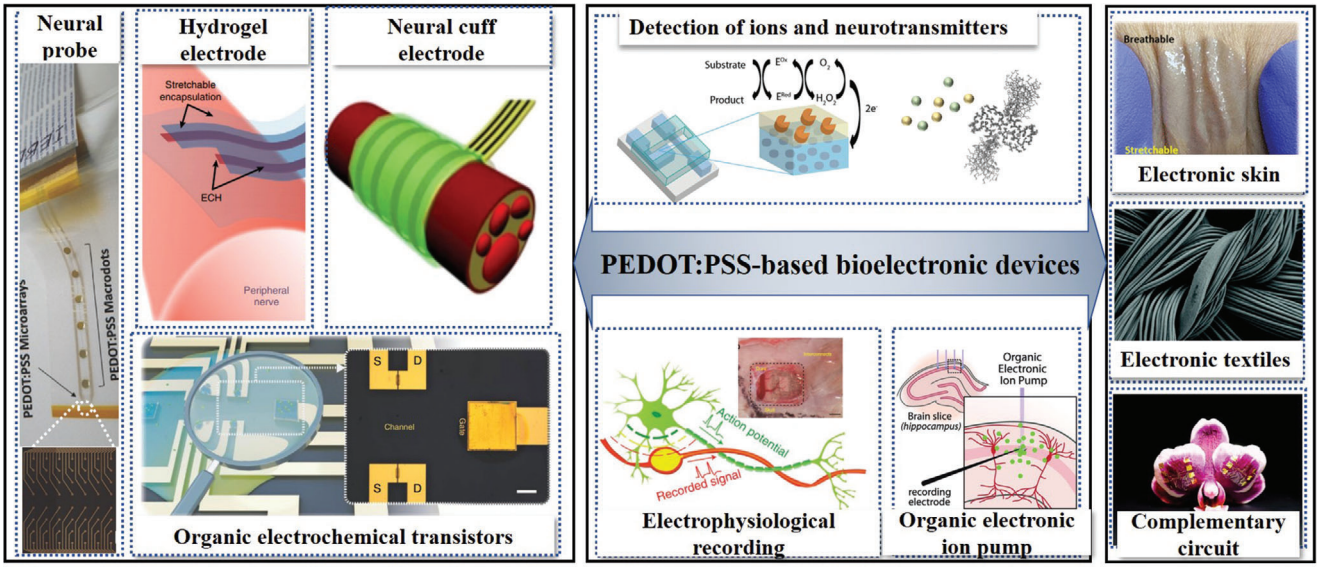

Figure 1. PEDOT:PSS-based bioelectronic devices in electrophysiological and biochemical applications: Left: representative PEDOT:PSS-based bioelectronic devices. Reproduced with permission.[24–27] Copyright 2017, Wiley-VCH GmbH. Middle: applications of these PEDOT:PSS-based devices for neurotransmitters detection, electrophysiological recordings, and modulation of biological activities. Reproduced with permission.[28] Copyright 2014, Wiley-VCH GmbH;[29] Copyright 2021, Wiley-VCH GmbH; [30] Copyright 2015, Wiley-VCH GmbH. Right: flexible and stretchable PEDOT:PSS-based devices used as electronic skin, electronic textile, and complementary circuit. Reproduced with permission.[31] Copyright 2021, American Chemical Society;[32] Copyright 2017, The Royal Society of Chemistry;[33] Copyright 2019, American Association for the Advancement of Science (AAAS).

with only a few millivolts in amplitude.[34] The postsynaptic (excitatory and inhibitory) inputs of various dendritic terminals are integrated by the neuron. If this signal exceeds a certain threshold potential, a full depolarization of the entire neuron is triggered. Both, the formation of a postsynaptic potential as well as the generation of action potentials involve the complex interplay of ionic and chemical stimuli predominantly regulating the electrophysiological activity of neurons. Consequently, the ideal bioelectronics sensors should be able of transducing these chemical and ionic signals with high sensitivity, specificity, and also high spatiotemporal resolution. The specific detection of the chemical processes on the cell (-membrane) usually requires a bioreceptor, which specifically interacts with the molecule of interest. Fundamentals and recent progress on PEDOT:PSS-based biosensors are discussed in more detail in Section 2.1 and Section 2.2. In the following, we will firstly focus on the transduction of the alteration of ion concentrations. At bottom, the high ion sensitivity of this material is due to the correlated ionic and electronic conductivity of its two mixed ionomers. Holes in π-conjugated $PEDOT^+$ domains are compensated by sulfonate anions of the insulating PSS molecules, which therefore act as dopants for the electronic conduction of the prior one. The PEDOT units adhere on PSS and thereafter form a tertiary structure (Figure 2c).[42] This effective doping facilitates an intrinsic conductivity of $\approx$1 S cm^{-1}, which is superior to most other reported organic conjugated polymers and can be improved even further to 4600 S cm^{-1} via mixing and/or post-treatment with organic solvents (e.g., ethylene glycol,[43] dimethyl sulfoxide,[44] methanol,[45] sorbitol[46]), surfactants (e.g., triton[47]), ionic liquids,[48] aqueous solutions of organic salts,[49] and organic or inorganic acids (e.g., sulfuric acid[50]). This dispersed 3D mixture of the cationic $PEDOT^+$ and the anionic PSS^- ionomers permits the inclusion of ions from the buffer medium, which can compensate intrinsic charges of the bulk polymer and affect the doping level as well as the electronic conduction. This doping/de-doping principle is used by the majority of PEDOT:PSS-based electrophysiological sensors, which are reviewed in the following sections.

2.1. Multi- or Microelectrodes: Recording and Stimulation

Multi- or MEAs have become one of the most commonly used extracellular recording and stimulation tools since their first application in recording of bioelectric activity in 1972.[69] They provide multiplexed, noninvasive recordings of extracellular field potentials with high temporal and spatial resolution.[70,71] The classic electrodes normally consist of metals such as gold, platinum, or iridium. The medium/metal interface functions as a transducer for the (ionic and chemical) signals elicited by adherent cells by conversion into electrical signals (current or potentials), which can further be registered by the amplifier electronics.[72] The mechanism by which the signal is picked up by the electronic system can be separated into two categories: i) the faradaic injection related to electrochemical reactions (oxidation or reduction) on the electrode surface and ii) the capacitive charge injection relying on charging and discharging of the electrochemical double layer at the medium/electrode interface.[72–74] Faradaic injections, associated with high recording electrode potentials, are usually undesirable (unless for neurotransmitter detection), since faradaic reactions may alter the chemical composition of the electrode or the electrolyte and could even cause the formation of toxic byproducts.[75,76] Therefore, electrode interfaces, which mainly rely on capacitive charge injection, are predominately used for the recording of electrophysiological signals.

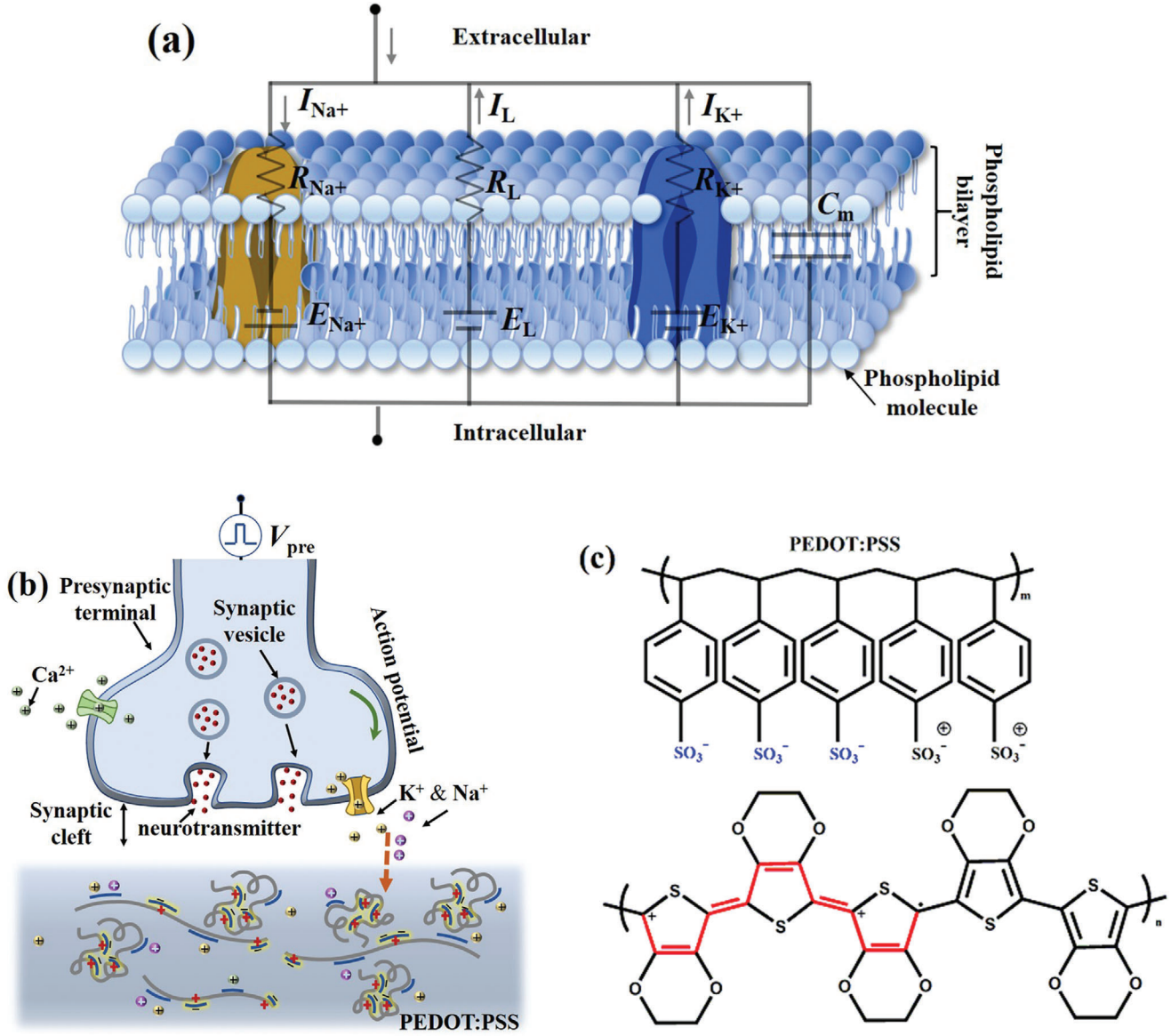

Figure 2. Interface between the cellular membrane and an organic bioelectronic device: a) The electrically equivalent circuit of the cellular membrane is based on the Hodgkin–Huxley model. b) Schematic of a biological synapse including the vesicle exocytosis and neurotransmitter release toward the synaptic cleft induced by an action potential arriving at the PEDOT:PSS terminal. The injection of cations in the organic film results in the de-doping of PEDOT (no shining yellow color). c) Chemical structure of polyethylene dioxythiophene: poly(styrene sulfonate) (PEDOT:PSS) sketching the partially doping of PEDOT (red) by PSS associated sulfonate groups and undoped domains due to a screening of the sulfonate charges by cations.

For a comprehensive investigation of the connectivity in neuronal networks, small-size and high-density probe systems are required (over 10 000 electrodes for in vitro MEA[77]), which, however, significantly increases the impedance of the individual electrodes, leading to poor cell-device coupling and small signal amplitudes.[11] Cogan highlighted a threshold charge density required for neural prostheses ranging from 0.05 to 4 mC cm^{-2}.[76] Therefore, to facilitate a low electrode impedance at small lateral footprint, a high charge injection capacity at the electrode interface should be maintained. Although applying high potentials on the electrode can enhance the capacitance (charging/discharging capability), faradaic processes such as water hydrolysis, electrode degradation, and tissue damage,[76,78] are unavoidable. Alternatively, increasing the capacitance by enlarging the effective surface area (porous or 3D electrode morphology) of the recording electrode raises the probability to pick up high amplitude signals. This approach is widely used in carbon-based electrodes;[60] however, this scaling effect is limited, and the electrode stability may suffer significantly. In 2003, Cui and Martin firstly proposed to coat electrodes by PEDOT:PSS via electrochemical deposition with the aim to reduce the senor impedance.[79] The polymer electrode had a charge injection limit value of 2.3 mC cm^{-2},[68] which was comparable to that of IrO_x and much higher than that for Pt electrodes, facilitating effective neural stimulation. **Table 1**

Table 1. The comparison of charge injection capability and volumetric capacitance of various electrode materials for cell stimulation and recordings. PtIr: platinum iridium, PBS: phosphate buffer saline, HepMA: heparin methacrylate.

	Charge injection capability [μC cm^{-2}]	Charge injection mechanism	Volumetric capacitance [F cm^{-3}]	Impedance [MΩ μm^2 at 1 kHz]	Electrolyte	Voltage [V]	Cell stimulation or recordings
Pt	100–150 (200 μs pulse)[51] in vitro: 54 (3200 μs) in vivo: 15.8[52,53]	Faradaic/ capacitive		3900	PBS	−0.6–0.9	[54]
Au	110[55,56]	Faradaic/ capacitive		2170	0.1 M KCl (2 × 10^{-3} M $K_3Fe(CN)_6$)	−0.6–0.8	[57]
Porous Au	1000	Faradaic/ capacitive		10.9	0.1 M KCl (1.0 × 10^{-3} M $K_4Fe(CN)_6/K_3Fe(CN)_6$)	−0.3–0.8	[58]
Graphene	3100[59]	Capacitive	376[60]	1364[55]	6 M KOH		[61]
Reduced graphene oxide	14.2 × 10^3	Capacitive		47.1	PBS	−1–0.9	[62]
CNT fibers	6.5 × 10^3	Capacitive		20.4	PBS	−0.6–0.8	[63]
PEDOT: PSS on PtIr	2.92 × 10^3	Faradaic		1.2	PBS	−0.6–0.8	[64]
PEDOT/CNT		Faradaic	39.3	24.3	NaCl		[65,66]
PEDOT/PVA-HepMA	68.4 × 10^3[52]	Faradaic			0.9% Saline	−0.7–0.7	
PEDOT:PSS	17.71 × 10^3[67]	Faradaic		107	"Ringer's solution"	−0.9–0.6	[68]
PEDOT:PSS/dopamine	6000	Faradaic		12.5	PBS	−0.6–0.8	[56]

summarized the charge injection capability and volumetric capacitance values of different electrode materials for cellular stimulation and recording, where PEDOT:PSS exhibits excellent capability for high capacitive charge injection compared to other electrode materials. An important feature of PEDOT:PSS for cell recordings is its volumetric capacitor characteristics, where the charge storing capability depends not only on the lateral dimensions, but also on the polymer layer thickness, yielding a capacitance per volume of $C^* = 39.3 \pm 1.3$ F cm^{-3}.[66] This value is roughly 100 times higher than the double layer capacitance of common metal electrodes. PEDOT:PSS as a volumetric conductor and capacitor has proven to be able to mediate the signal transmission between cells and electronics in various device configurations. Recently, PEDOT:PSS has exerted its capability to minimize the impedance of MEAs without scarifying the electrode density.[80]

Various deposition methods have been established to decorate the electrode surfaces with this polymer for wafer-scale fabrication including spin/blade-coating (**Figure 3**a)[81] or in situ electropolymerization from its monomer solution.[82] Sessolo et al. found that the impedance of PEDOT:PSS-based MEA was one order of magnitude lower than that of the bare-Au MEA (Figure 3b),[81] which was partly ascribed to the increased electrode surface area caused by the high porosity of PEDOT:PSS.[83] The lower impedance gave rise to improved recordings from hippocampal slices with a higher signal-to-noise ratio (S/N ratio).[81] Liu et al. fabricated a soft 3D micropillar electrode array composed of a conductive hydrogel, which was obtained from PEDOT:PSS-modified by an ionic liquid (4-(3-butyl-1-imidazolio)-1-butanesulfonic acid triflate). This polymer electrode material exhibited approximately tenfold higher signal-to-noise ratio (S/N = 33.7) for cardiomyocyte recordings compared to iridium oxide micropillars (S/N = 3.1) due to an overall reduction of the electrode impedance by PEDOT:PSS.[84] Zips et al. blended PEDOT:PSS with multi-walled carbon nanotubes (MWCNT) to formulate an ink, which was later on used to print arrays of needle-like electrodes with a height of 33 ± 4 μm and a diameter of 10 ± 2 μm by a combined aerosol-jet and inkjet printing process (Figure 3c). The PEDOT:PSS/MWCNT composite not only possessed a high mechanical strength but also a high conductivity (323 ± 75 S m^{-1}) facilitating a low impedance at a frequency of 1 kHz and thus a high S/N ratio of 24 for recording cardiomyocyte-like HL-1 cells.[85] Other works reported the doping of PEDOT during the electrochemical deposition with other materials such as dopamine[56,80] and carbon nanotubes[86] with the aim to decrease the impedance of the electrodes, as well.

2.1.1. Neural Pixel

To understand the coordinated activity of large neuronal populations, it is critical to record signals from multiple brain regions continuously over hours, weeks and months, which requires electrode arrays with high spatial and temporal resolution.[4,88] Recently, Jun et al. developed a silicon-based device named as neuro pixel, which had 384 recording channels and 960 programmable sites, enabling the simultaneous recording of the activity of neural tissue on numerous sites while changing the position of the recording without relocation of the probe inside the animal.[70] Given the mechanical mismatch between conventional Si-based device and the tissue, which limits the chronic use in human due to the unavoidable neural damage, neuro pixel based on organic

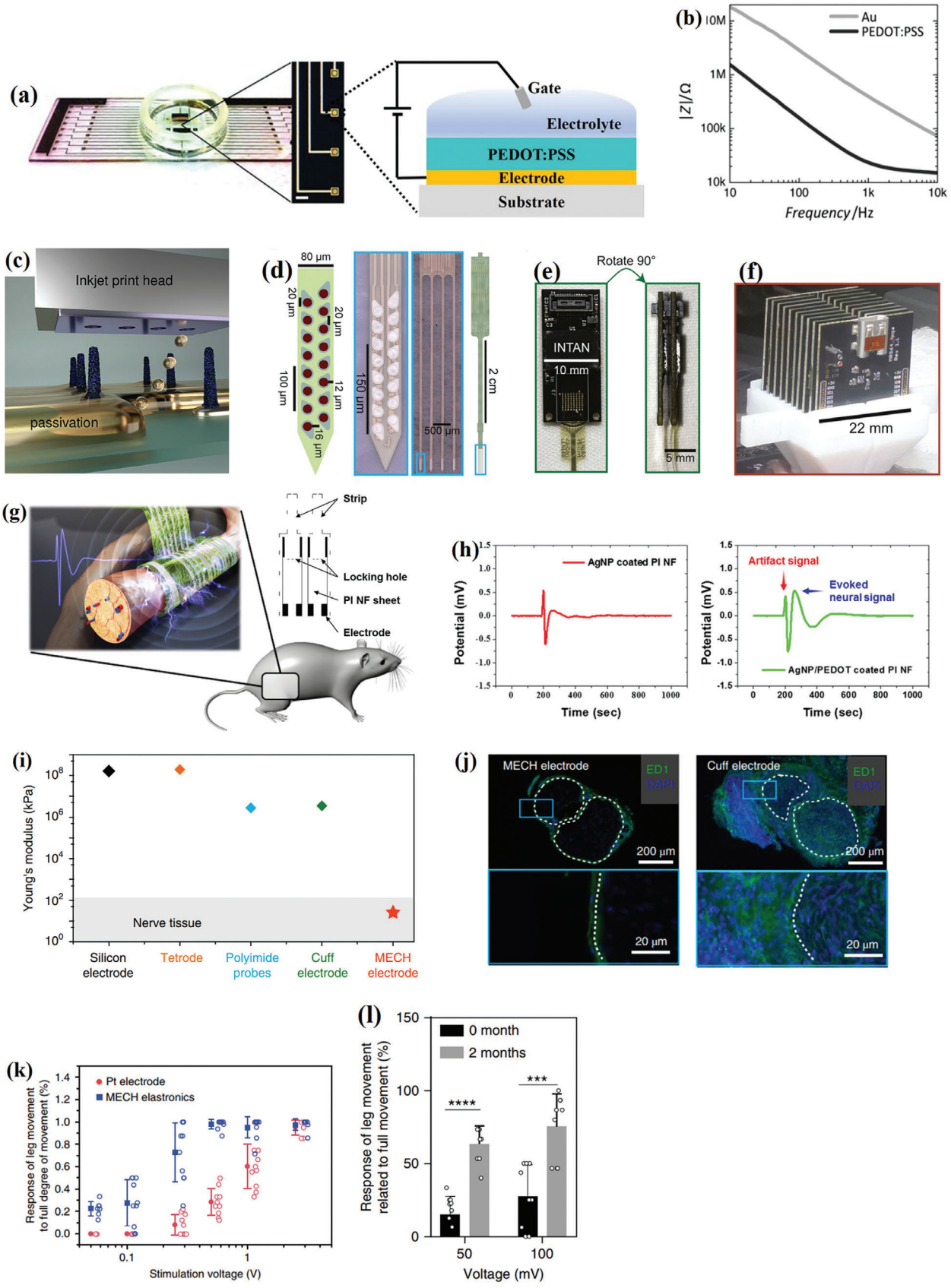

conducting polymer may become a promising alternative.[89] To this end, Chung et al. developed multi-shank polyimide electrode arrays on silicon stiffeners for recording neuronal activity (Figure 3d). The recording contacts consisted of a platinum electrode covered by electrodeposited PEDOT:PSS, which were bonded on a circuit board (Figure 3e).[4] The obtained device featured 1024 channel electrodes, similar as the reported silicon-based neuro pixel (Figure 3f), which could measure the activity of large populations of individual neurons and supported a continuous recording, yielding high-quality recordings for at least 5 months.[4] Therefore, it could be speculated that the soft neuropixel is a suitable tool to acquire information about the brain connectivity and facilitate further development of brain–machine interfaces.

2.1.2. Implantable Neural Cuff Electrodes

Interfacing neurons of the peripheral nervous system require electrodes featuring a conformal contact to the nerve fiber, providing selective recording from and stimulation of independent single or multiple neuronal cells. Since its first implantation in nerves in 1985, cuff electrodes have developed into a widely used tool for site-specific drug administration and electrical stimulation and recording.[90] As a type of extracellular neural electrode, it completely covers the nerve trunk[91] causing minimal tissue damage, and thus allowing longer neural communication.[87,92] Although the cuff electrode is a noninvasive nerve electrode, its stiff structure could provoke serious adverse reactions such as inflammation, blood vessel compression, and neurological atrophy. To overcome these challenges, researchers attempted to developed minimally invasive and biocompatible electrodes mainly from two major avenues. One is using softer materials (e.g., polyimide, parylene C, polydimethylsiloxane (PDMS)) instead of the traditional silicone-based substrates. The other one is manipulating the electrode design, e.g., C-shape,[93] self-locking with a strip and locking loop[94] to minimize the compression and discomfort of the tissue. Besides these two strategies, surface modification and coating of the electrodes with drugs, polymers, or anti-inflammatory biomolecules are complementary approaches to reduce the mechanical mismatch and prevent inflammation. Coating the electrode with conducting polymers (e.g., PEDOT:PSS) permits the neural electrode to fully conform to the nerve trunk, thus facilitating the recording of high-quality nerve signals. Heo et al. reported on a micro-well cuff electrode, which was coated with a polyethylene glycol hydrogel, drug loaded poly(lactic-*co*-glycolic) acid microspheres, and PEDOT:PSS. The obtained electrodes exhibited a sustained release of drugs while the hydrogel/PEDOT:PSS surface coating significantly decreased the fibrous tissue deposition and improved the communication between tissue and electrode, enabling high-quality nerve signals.[92] In a follow up work, they developed a polyimide (PI) nanofiber-based nerve electrode utilizing silver nanoparticles as electrode connection pad and PEDOT:PSS as the conductive layer for recording long-term stable neuronal signals (Figure 3g). They found that the involvement of electropolymerized PEDOT:PSS could significantly improve the charge injection capacity of the cuff electrode due to the enlarged active surface area caused by the conductive polymer, facilitating higher amplitudes for the transmitted signals compared to electrodes without PEDOT:PSS (Figure 3h). In addition, the PI nanofiber-based nerve electrodes had a smaller contact area with the neural tissue than the PI film-based electrodes, thus reducing the shrinkage of the nerve tissue resulting from its compression of the electrode. Consequently, the fiber-based electrode enabled stable recordings of electroneurograms for 12 weeks.[87] The implementation of PEDOT:PSS as coating or matrix material proofs to be beneficial for the development of cuff electrodes due to the improvement of the signal recording performance and the suppression of immune responses of the investigated neural tissue. Thus, PEDOT:PSS-based hydrogels appear to be well suited as nonamplifying, capacitive coupling element in the field of neural tissue engineering.

2.1.3. Conductive Hydrogel-Based Electrodes

Although the nominal impedance of an electrode could be remarkably reduced by the coating with PEDOT:PSS, adverse biomechanical interactions between the electrode materials and the target tissue, especially for implantable devices, could increase the interfacial impedance and electrode-tissue cleft due to immunoreactions, thus hampering the performance of bioelectronics during stimulation and recordings.[72] The mechanical mismatch of the two systems mainly originates from their significant difference in the Young's modulus. Compared with the moduli of neural tissues (≈10 kPa), conventional electrode materials, such as silicon, platinum, or gold, exhibit extremely high

Figure 3. PEDOT:PSS modified microelectrode array for recording cell signals: a) The photograph of a multi-electrode array with an in vitro culture chamber ring attached on top. The scale bar is 10 µm. On the right side the schematic illustration of a PEDOT:PSS-coated electrode and the wiring diagram for operation are shown. b) A comparison of the impedance magnitude $|Z|$ versus the frequency for a PEDOT:PSS coated electrode and a gold electrode. Reproduced with permission.[81] Copyright 2013, Wiley-VCH. c) Aerosol- and inkjet printed needle-shaped electrode tips coated by a PEDOT:PSS composite doped with multi-wall carbon nanotubes (MWCNTs). Reproduced with permission.[85] Copyright 2019, American Chemical Society. d) Polymer-based electrode array. Left: schematic illustration of a 16-channel shank with an electrode diameter of 20 µm and electrode-to-electrode distance of 20 µm. Middle: Optical image of the 16-channel array polymer-based shank (middle left) and four shanks with 64-channel array (middle right). e) Left: Individual 64-channel shank module comprising an amplifying, multiplexing, and digitizing chip wire bonded onto a board, which has an attached mezzanine-style connector on top. Right: Side view of two stacked modules. f) 16 stacked modules with a 1024-channel array in an FPGA headstage during implantation. Reproduced with permission.[4] Copyright 2019, Elsevier. g) Schematic illustration of the construction of the cuff electrode and its application in recording neuronal signals. h) Acute ex vivo recordings of neuronal signal using a silver nanoparticles (AgNP)-coated nanofiber electrode (top) and an AgNP/PEDOT:PSS-coated electrode (bottom). Reproduced with permission.[87] Copyright 2017, American Chemical Society. i) Comparison of the Young's modulus of a conductive hydrogel electrodes and conventional implantable cuff electrodes. j) Cross-section slice of a sciatic nerve of a rat labelled by the inflammatory biomarker ED1 for the MECH electrode and the cuff electrode. k) The percentage of leg movement with respect to the full degree of movement under different stimulation voltages for the MECH electrode and the platinum electrode with the same exposed area ($n = 9$). l) After 2 months of soaking in PBS, the MECH electrodes stimulated and even higher percentage of leg movement with respect to the full degree of movement at 50 and 100 mV, respectively. Reproduced with permission.[25] Copyright 2019, Springer Nature.

Young's moduli over 1 GPa.[20] Even state-of-art dry polymers, e.g., polyimide, polycarbonate, PET, and pristine PEDOT:PSS exhibit elastic moduli as high as 100 MPa to 10 GPa.[95] In contrast, hydrogels possess tissue-like mechanical properties (<100 kPa) and have therefore been used to decrease in the mechanical mismatch.[96] Furthermore, hydrogels formed from conducting polymers facilitate ionic and electronic conductivity as well as tunable mechanical and chemical properties. The intrinsic water-rich nature of conductive polymer hydrogels facilitates the transport of biological and chemical molecules, thus providing an extracellular matrix-like environment and rendering them as one of the most promising materials in the emerging field of hydrogel bioelectronics.[97] PEDOT:PSS is a widely used conducting polymer hydrogels due to the hygroscopic properties of PSS and its favorable cytocompatibility, because a hydrogel can directly be formed from PEDOT:PSS simply by adding ions.[98] At a low sorption degree, the uptake of water molecules mainly occurs via the hydrophilic sulfonic acid groups. With increasing sorption degree, these active sites become occupied and unbound water molecules exist in a free-movable configuration. The water molecules incorporated into the PEDOT:PSS increase the distance between their grains, leading to larger film volumes and the formation of hydrogel characteristics,[99] which, however, is accompanied by a decrease in electrical conductivity and enhancement in neuroinflammatory responses due to the increased contact area with tissue. These drawbacks may result in the reduction in stimulation/recording efficacy and hamper the miniaturization of the soft electronics and their applications for precise neuromodulation in vivo.[100] Over the past years, plenty of methods have been developed to achieve high-conductivity PEDOT:PSS-based hydrogel without sacrificing their physicochemical properties, including in situ polymerization or mixing of the conducting polymer within nonconductive hydrogels to form interpenetrating polymer networks (IPN), blending PEDOT:PSS with conductive nanofillers (e.g., metal nanoparticles/wires, carbon nanotubes, or graphene) .[101] For example, Yao et al. prepared a hydrogel by treating a PEDOT:PSS suspension with sulfuric acid (H_2SO_4) at 90 °C for 3 h followed by a repeated washing with deionized water. The resulting hydrogel had an extremely high electrical conductivity of 880 S cm^{-1}, which could be attributed to the extraction of insulating excess PSS and the formation of a porous fibril structure of PEDOT.[102] However, the H_2SO_4-assisted post-treatment suffers from several drawbacks, such as safety and environment concerns and the acidic residues may somehow limit its applications.[103] Lu et al. developed a high-performance hydrogel by mixing PEDOT:PSS with dimethyl sulfoxide (13 vol%) and applied a dry-annealing (three times annealing for 30 min at 130 °C) and rehydration post-treatment.[104] The obtained pure PEDOT:PSS hydrogel exhibited a low Young's modulus of ≈2 MPa and a relatively high conductivity (≈20 S cm^{-1} in phosphate buffer and ≈40 S cm^{-1} in deionized water) due to the formation of PEDOT:PSS nanofibrils. Liu et al. fabricated a soft and elastic hydrogel-based microelectronic device via exchanging the ionic liquid additive in PEDOT:PSS with water[25] and employing an elastic fluorinated photoresist as passivation layer. The obtained conductive hydrogel electrode not only featured ionic and electronic conductivity, but also had a Young's modulus value of ≈32 kPa in the range as nerve tissue (Figure 3i). Thus, different from Au-PET electrodes, which induced significant growth of inflammatory tissue around the nerve bundles (Figure 3j, right), only minimal inflammatory tissue growth was induced by the hydrogel electrode (Figure 3j, left). In addition, the hydrogel electrode was successfully employed to record intramuscular electromyogram traces at low stimulation voltages of 50 mV while a voltage of 500 mV was required for the corresponding Pt electrode (Figure 3k).[25,104] A long-term electrochemical stability of the conductive hydrogel was validated by soaking the electrode in PBS for 2 months without the decay in leg response (Figure 3l). A broader overview on earlier reported PEDOT:PSS hydrogel works and their application in bioelectronics can be obtained from previous comprehensive reviews.[72,105] All in all, tuning the swelling properties of PEDOT:PSS-based hydrogels by physical and chemical treatments facilitates the tailoring of compliant mechanical properties while maintaining their electrical characteristics, which provides promising prospects to reduce the immune response and to accommodate body movements while wearing implantable devices.

2.2. Organic Electrochemical Transistors

OECTs, firstly described in 1984 by White et al.,[106] have exerted their merits as promising bioelectronic device type for applications such as neural recording elements, biomolecule sensors, cellular sensors, and as the constituent component for bioinspired, neuromorphic interfaces.[107,108] Different from the capacitive coupling sensors reported in the previous paragraphs, OECTs have the advantage that the measured current signals can be effectively modulated by very low gate voltages exerted to the polymer channel (below 1 mV) resulting in a high signal amplification.[109] OECTs are typically operated in a three-terminal configuration where a polymer channel is defined by source and drain electrodes, while the liquid-gate electrode is connected to the device via an electrolyte solution contacting the organic channel. Commonly, the source contact is grounded in this device configuration and a bias voltage is applied to the drain contact relative to the ground. Unlike the conventional field-effect transistors, which use an insulating gate oxide separating the channel from the electrolyte and prohibiting an ion exchange across the solid-liquid interface, the organic channel of an OECT can direct contact and communicate with the electrolyte. In the early years, different organic semiconductors have been utilized as channel materials for OECTs, such as polypyrrole and polyaniline. Since 2016, PEDOT derivatives, glycolated semiconducting polymers, and n-type organic semiconductors were used.[110] Numerous publications in various fields suggest that PEDOT:PSS is the most successful channel material for state-of-the-art OECTs mainly due to its commercial availability, high conductivity and transparency, excellent processability, and biocompatibility. The mixed ionic/electronic conductivity and the swelling properties of PEDOT:PSS in aqueous solution endow it with the capability to enable a rapid penetration and extraction of ions toward or from the polymer channel.[111] The penetration of ions into the channel of OECTs determines the time response of the device rather than the accumulation at the sensor surface.[66,112] OECTs can be considered as a combination of an ionic and an electronic circuit (**Figure 4**a). The electronic circuit describes the transport of charge carrier (holes/electrons) in the polymer material that bridges the

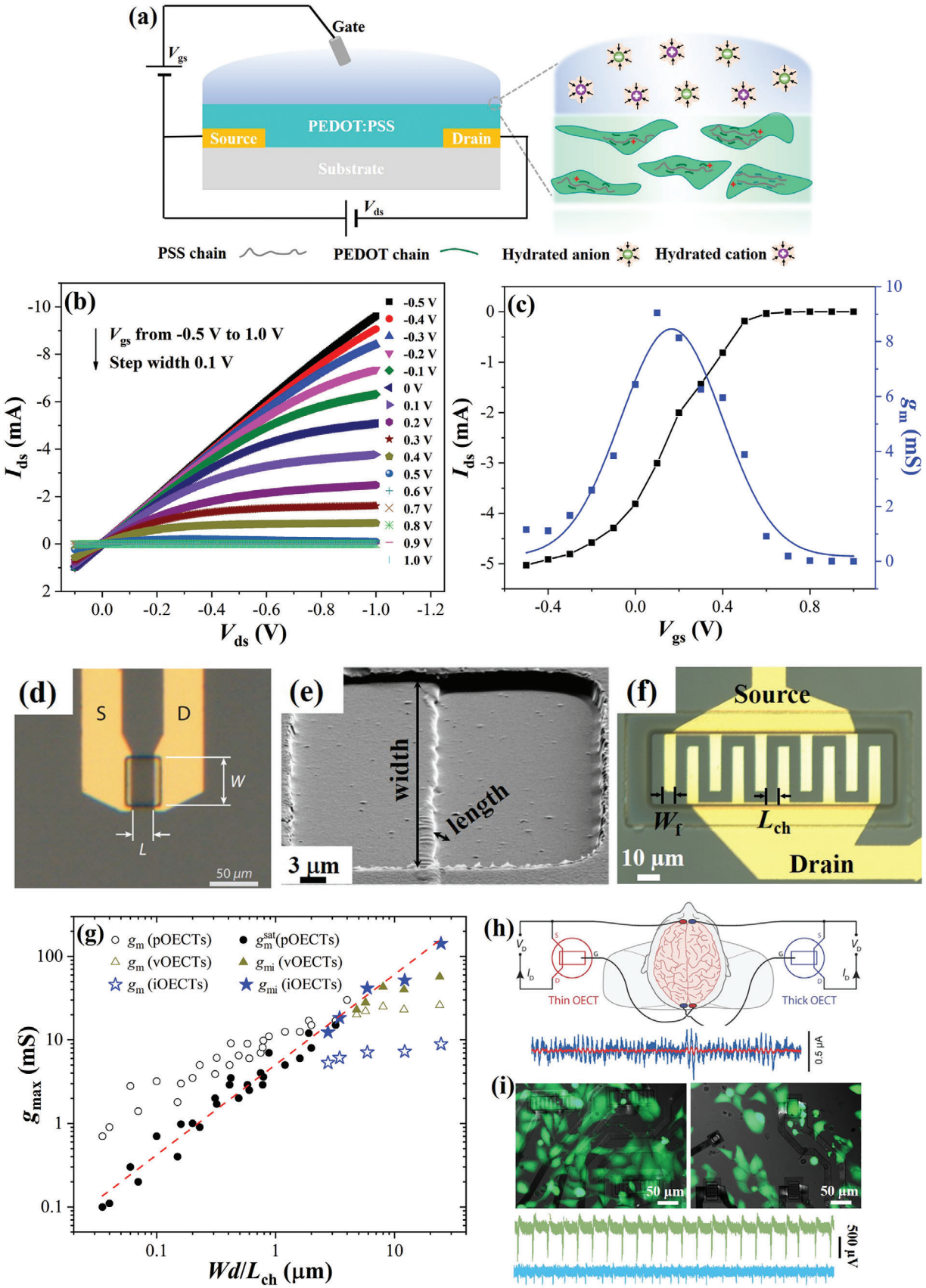

source and drain electrodes and can simply be modeled by Ohm's law. Consequently, the transport time of charge carriers in the organic channel is mainly dependent on their mobility. The ionic circuit is typically characterized via a more complex equivalent circuitry comprising the electrolyte resistance (R_s) as well as parallel capacitors/resistor elements (R_C) for the gate/electrolyte (C_g) and electrolyte/channel (C_{ch}) interfaces in series. Regarding their operation mode, OECTs can be divided into depletion and accumulation mode devices. PEDOT:PSS-based OECTs typically work in the depletion mode. Once a positive bias is applied to the gate electrode, an electrical double layer is formed. The anions accumulate around the gate electrode, while the cations from the electrolyte penetrate into the polymer channel and compensate the pendant sulfonate anions of PSS, leading to a de-doping of PEDOT. Thus, a decrease of the source–drain current (I_{ds}) is observed (Figure 4b) corresponding to a depletion of charge carriers, which finally leads to the OFF state of the device (Figure 4c).[107] The OECT operation can be considered as an "electrochemical doping" process, where a de-doping of PEDOT occurs due to an electrochemical reaction, described as follows:[113]

$$\mathrm{PEDOT^+ : PSS^- + M^+ + e^- \rightleftharpoons PEDOT + PSS^- : M^+} \quad (1)$$

where M^+ represents cations from the electrolyte and e^- stands for electrons from source electrode. It can be concluded that the electrochemical doping process is partially governed by the mobility of the ions. Stavrinidou et al. developed a planar electrolyte/PEDOT:PSS junction to straightforwardly evaluate the ion drift mobility. They found that the mobility was different from each other for several ions (H^+, K^+, Na^+) in PEDOT:PSS and higher than their electrophoretic mobility in bulk water. This results in ion-selective characteristics of OECT device, which has interesting implications for applications of PEDOT:PSS to interface electrogenic cells.[114]

It is widely accepted that the seal resistance strongly influences the efficiency of the channel gating. The seal resistance itself depends on the interfacial cleft between the cellular membrane and the device as well as coverage of the channel area (lateral sealing) by the cell. The dimensions of the channel areas effect the lateral sealing and thus also the coupled voltage, resulting in variations of the output channel current. If the channel area exceeds the contact area to the cell significantly, large parts of the channel remain unaffected by the potential variation of the membrane potential and the recorded signal is overlaid by interfering noise. Reducing the device dimensions on the other hand can strongly impair the device sensitivity. This contradiction challenges the development of OECTs that are capable to record action potentials from individual cells and requires a careful sensor design. The figure of merit that determines the capability to convert the input gate voltage signals into a measurable variation of the output currents across the PEDOT:PSS channel is termed as transconductance (g).[43] Recently, strong efforts were done to improve the transconductance for PEDOT:PSS-based OECTs. To this end, OECT devices with different channel geometries were developed (Figure 4d–f). Rivnay et al. found that the maximum transconductance (≈2 mS) could be achieved at zero gate bias by tuning the width-to-length ratio of the organic channel (W/L_{ch}) for planar OECTs (pOECTs) and demonstrated that the transconductance is governed by this W/L_{ch} ratio rather than the channel area (Figure 4d).[115]

Donahue et al. developed vertical OECTs (vOECTs), which had a channel length down to 450 nm, resulting in a significant improvement of the maximum transconductance up to 25 mS (d = 180 nm) (Figure 4e).[116] Our previous work reports on interdigitated OECTs (iOECTs), which could remarkably improve the W/L_{ch} ratio without sacrificing the transistor density. We found that apart from W/L_{ch} ratio, the channel resistance and source–drain series resistance between PEDOT:PSS and Au electrode strongly affect the transconductance. While the channel resistances primarily depend on the distance between two adjacent electrodes, the source–drain series resistance is governed by the electrode width (Figure 4f).[117]

Apart from the W/L_{ch} ratio, the channel thickness (d) plays a crucial role in the device transconductance as well,[66] which is a clear difference to that of organic field-effect transistors (OFETs).[118] The volumetric nature of the capacitance results in a dependence of the peak transconductance on the 3D geometry of the device (Figure 4g), which could be written as follows

$$g_m = \left(Wd/L_{ch}\right)\ \mu C^* \left(V_T - V_g\right) \quad (2)$$

where μ is the mobility of charge carrier, V_g the gate potential, d the polymer layer thickness, C^* the capacitance, and V_T is the threshold voltage. For OFETs, its transconductance is described by replacing $d \times C^*$ in Equation (2) by the per unit area capacitance C_i, indicating that g relies on the interfacial enrichment of ionic charges and is only limited by the capacitance of the double layer.[118] Differently, given the volumetric response of the capacitance for OECTs, ions interact with the entire volume of the polymer channel, resulting in OECTs with higher transconductance than other electrolyte-gated transistors, and making OECTs an ideal candidate for the recording of cellular signals.[119,120]

Figure 4. Electrical performance of organic electrochemical transistor (OECT). a) The schematic view of the cross-section of an OECT and the wiring diagram for the device operation. The enlarged image indicates the interface between electrolyte and organic channel material PEDOT:PSS and the red cross represents holes in the PEDOT chain. b) The output characteristics of OECTs recorded by varying gate-source voltages (V_{gs}) from −0.5 to 1.0 V with a step of 0.1 V. c) The extracted transfer characteristics and corresponding transconductance values, when the drain–source voltage (V_{ds}) equals to −0.5 V. Reproduced with permission.[117] Copyright 2019, Wiley-VCH GmbH. d) The micrograph of planar OECTs (pOECTs). Reproduced with permission.[43] Copyright 2013, Wiley-VCH GmbH. e) The SEM image of vertical OECTs (vOECTs). Reproduced with permission.[116] Copyright 2018, Wiley-VCH GmbH. f) The micrograph of interdigitated OECTs (iOECTs). g) The comparison of the maximum transconductance as a function of Wd/L for three different OECTs shown in (d–f). Reproduced with permission.[117] Copyright 2019, Wiley-VCH GmbH. The influence of the channel geometry for PEDOT:PSS-based OECTs to the recording electrophysiological signals. h) Top: Wiring diagram of two OECTs with different thicknesses of the active layer, which were simultaneously used as transducers to record human electroencephalography (EEG) signals. Bottom: The corresponding EEG signals recorded by thick OECT (blue, 870 nm) and thin OECT (red, 230 nm), respectively. Reproduced with permission.[66] Copyright 2015, AAAS. i) The morphology of cardiomyocyte-like HL-1 cells stained with calcein-AM on big channel OECT (channel area of 57 μm × 26 μm, left) and small channel OECT (30 μm × 22 μm, right) as well as the action potential spikes of HL-1 cells recorded by big channel OECT (green) and small channel OECT (blue), respectively. Reproduced with permission.[117] Copyright 2019, Wiley-VCH GmbH.

Normally, electrophysiological signals can be measured by transistors according to the equation: $V_{gate} = \frac{V_{out}}{g_m \times FBR}$, where FBR is the feedback resistance and $g_m \times FBR$ indicates the preamplification factor of the device in a transimpedance amplifier circuit.[117] A higher transconductance can therefore lead to higher signal amplitudes. For example, Rivnay et al. utilized OECTs with two different PEDOT:PSS layer thicknesses as channel (Figure 4h) and found that the thick-channel OECT with higher g_m exhibited more distinct EEG traces in comparison with the thin channel device.[66] In our previous work, we compared two iOECTs with different channel geometries and demonstrated that the channel with higher transconductance (due to the lower channel and source–drain series resistances) showed a higher signal-to-noise ratio (≈18) for the recording of action potentials compared to the one with a small channel (≈2–5) (Figure 4i).[117] Correspondingly, the recording of extracellular signals from individual cells can be achieved if high-performance OECTs with large transconductances are developed that feature cell dimensions at short channel widths, wide channel lengths, low source–drain series resistance, and preferably high layer thickness.

However, besides the channel geometry-related transconductance, the response time of a device is also of great importance for monitoring rapid biological events, which are in the kHz range for action potentials. The response time of the sensor can be determined by fitting the drain current transient induced by a gate voltage pulse. It was proposed that the volumetric capacitance not only affects the transconductance but also influences the dependence of the response time on the channel geometry.[66] The response time (τ) of an OECT device is determined by both the electronic (τ_e) and the ionic transit time. The former can be described by $\tau_e = L_{ch}^2/\mu V_{ds}$ and extracted by plotting the slope of the source–drain transit as a function of the applied gate current.[107] For interdigitated OECTs, τ_e was linearly correlated to the electrode pitch, which includes both the channel length L_{ch} and the width of the electrodes W_f. Interestingly, a transition from the iOECT to the pOECT characteristics was observed at a transistor with pitch size of 10 µm, where τ_e of the iOECTs decreases and converges that of pOECTs (**Figure 5**a).[117] It has been reported by Rivnay et al. that holes in PEDOT:PSS-based OECT channels have an average mobility of 1.9 ± 1.3 $cm^2\ V^{-1}\ s^{-1}$,[66] which is about three orders of magnitude higher than the ion mobility in water. Thus, it is the ionic transit time that governs the device response time, which is described as $\tau_i = C_d\ R_s$, where C_d is linearly dependent on the channel area and R_s is the solution resistance.[121] A previous study showed that the response time is thickness-dependent due to the volumetric response of the capacitance of the OECTs,[66] which means that a high transconductance resulting from a high channel thickness comes on the costs of a rather slow operation.[122]

In a very recent study, we demonstrated micro-scale OECTs based on very thin (10–20 nm) PEDOT:PSS with bandwidth up to 10 kHz. The devices were used to impedimetrically measure the cell-substrate adhesion of individual cells by characterizing the transistor-transfer function. In this measurement technique, OECTs are brought into a working point by applying constant drain–source and gate-source voltages, while the bandwidth of the OECT plus transimpedance amplifier is measured by applying a small sinusoidal stimulation voltage at the gate electrode. Attachment and adhesion of individual cells as well as blocking of gap junctions between several cells can be recorded by this novel technique.[123]

For even faster response times of the OECTs, Spyropoulos et al. developed an internal ion-gated OECT (IGT) (Figure 5b), by adding D-sorbitol to PEDOT:PSS to create an "ion reservoir" within the polymer channel, which reduced the response time of the device and facilitated the operation in depletion mode. In this operation mode, the unbiased transistors show a high channel conductivity. However, the application of a positive gate voltage induces that the mobile ions diffuse toward PSS^- and compensate their sulfonate anions, which eliminates the doping effect and diminishes the channel current. Due to the fast (de-)doping process of the IGT, the novel device yielded an ultralow time constant of 2.6 µs (IGT device with W = 5 µm, L_{ch} = 12 µm, Figure 5c) without sacrificing the high device transconductance (g_m = 32.3 mS, device with W = 500 µm, L_{ch} = 5 µm, operated at V_{ds} = −0.6 V) and enabled higher frequency operation (380 kHz of effective bandwidth) (Figure 5d).[33] Their further work reports on an accumulation-mode IGT (e-IGT). The conversion of the operation mode was achieved by the addition of the polycation polyethylenimine (PEI) to the PEDOT:PSS/D-sorbitol channel materials. In the initial off state (V_{gs} = 0 V), PEDOT is in its reduced state ($PEDOT^0$) due to an electron transfer from the amine groups of PEI to PEDOT:PSS. The protonated PEI^+ established ionic bonds with PSS^- to balance the charges (Figure 5e, top). When a negative gate bias was applied (Figure 5e, bottom), the cationic charge of PEI^+ could be compensated, which led to a dissociation of the bound PSS and recombined subsequently with PEDOT leading to an increased channel current.[124] In contrast to other organic electrochemical devices, whose operation speed were dominated by ion mobility (10^{-2}–10^{-4} $cm^2\ V^{-1}\ s^{-1}$), the e-IGT architecture could leverage a higher hole mobility of PEDOT:PSS to increase the operation speed of the device (0.1–10 $cm^2\ V^{-1}\ s^{-1}$) (Figure 5f).[43,125–127] These findings demonstrated the versatility of PEDOT:PSS in modulating the transistor operation mode by alternating the channel composition, which could significantly extend the application of OECTs in complementary circuits in future.

To conclude this section, the bio-tissue like ionic conduction of PEDOT:PSS, its electrical, mechanical, thermal stability (high steam pressure at 121 °C for several minutes for sterilization is possible) ,[128] the bio-functional versatility, as well as its ion selectivity,[129] and signal amplification capability make OECTs an ideal candidate for in vivo and in vitro monitoring of electrophysiological signals.

3. The Applications of PEDOT:PSS-Based Bioelectronic Devices

3.1. Channel and Gate Modified Biochemical OECT Sensors

OECTs are particularly suitable for biological sensing applications because the devices can operate in aqueous solutions. As mentioned above, the transmission of action potentials is mainly regulated by ions and neurotransmitters. Even small deviations of their concentrations from the physiological level can be associated with pathological states.[41] The recognition of disease-related abnormalities in their expression or the detection of specific biomarkers at an early disease stage supports the timely

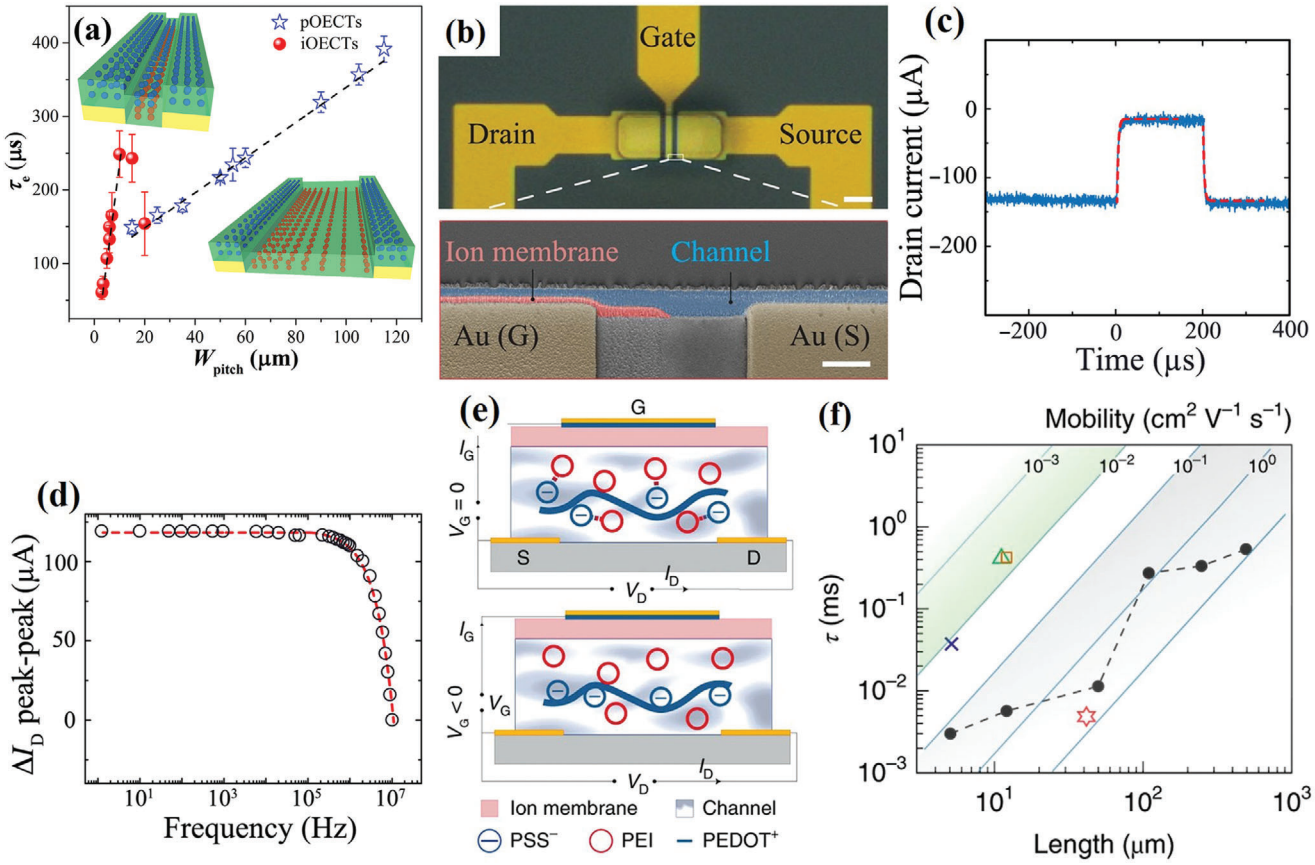

Figure 5. Response time of PEDOT:PSS-based OECTs with different architectures. a) The time-of-flight of pOECTs and iOECTs with different channel geometries. Reproduced with permission.[117] Copyright 2019, Wiley-VCH GmbH. b) Optical micrograph representing the top view of an internal ion-gated OECT (IGT). The scale bar is 20 μm. The enlarged scanning electron microscopy image depicts the cross section of the device. The optical micrograph displays the top view of an individual transistor. c) Temporal response of I_{ds} for an IGT device with width $W = 5$ μm and length $L = 12$ μm. Fitting of the IGT drain current (red) delivers a time constant of 2.6 μs. d) Frequency response of small-signal peak-to-peak drain current of an IGT device obtained by applying 100 mV peak-to-peak sine wave at the gate bias at $V_{ds} = -0.6$ V. Reproduced with permission.[33] Copyright 2019, AAAS. e) Schematic illustration of the cross section for an enhancement-mode, ion-gated transistor (e-IGT) and the wiring diagram of the device. The top one indicates the operation of the e-IGT at $V_{gs} = 0$ V, when PEDOT was in its reduced state, while the bottom one describes the state of the PEDOT:PSS channel under a negative applied gate voltage. f) Comparison of rise time between the PEDOT:PSS-based e-IGT device, which is governed by hole mobility (black circles) and other ion-based transistors determined by ion mobility (star, cross, triangle, and rectangle) with different channel length. The poly-Si-based e-IGT (star) falls in the hole-mobility regime. Reproduced with permission.[124] Copyright 2020, Springer Nature.

diagnosis and permits the monitoring of disease progression, which facilitates the treatment, improves potentially the prognosis, and reduce mortality. Biosensors capable of detecting neurochemicals at minute amounts in body fluids can indicate emerging neurological illnesses and surveil biomarker levels at point-of-care for chronic diseases. Two functional components are determining the performance of biosensors in terms of sensitivity and selectivity. One is responsible for signal conversion (transducer) and the other is in charge of target recognition (receptor) (**Figure 6**a).

The most commonly employed bio-receptors for electrochemical sensors applications are antibodies, enzymes,[130] selective membranes, and aptamers.[131] All of these recognition elements have been implemented in PEDOT:PSS-based electrochemical transducers and plenty of highly sensitive electrochemical biosensors have been obtained for the detection of metabolites, biomarkers, and ions. Kumar et al. fabricated a low-cost biosensor for the detection of a cancer biomarker (carcinoembryonic antigen) by using electrospun PEDOT:PSS/polyvinyl alcohol nanofiber decorated conducting paper as the amperometric transducer and carcinoembryonic antibodies as recognition element. The obtained biosensor exhibited high sensitivity (14.2 μA ng^{-1} mL cm^{-2}) and stability (22 days) due to the large number of biochemical interaction sites on the nanofibers and the excellent electrochemical properties of PEDOT:PSS.[132] Antibody detection assays have been established for numerous acute and chronic neuroinjury and neurodegenerative biomarkers, however OECT-based sensors utilizing these antibody receptors are still rare.[133–136]

Nevertheless, integrating biomolecules such as bioreceptors in micro- and nanotechnological components, which act as signal transducer, holds great promise to provide biosensor devices that support a minimally invasive, rapid, and precise diagnosis by the physician and permit point-of-care disease surveillance.

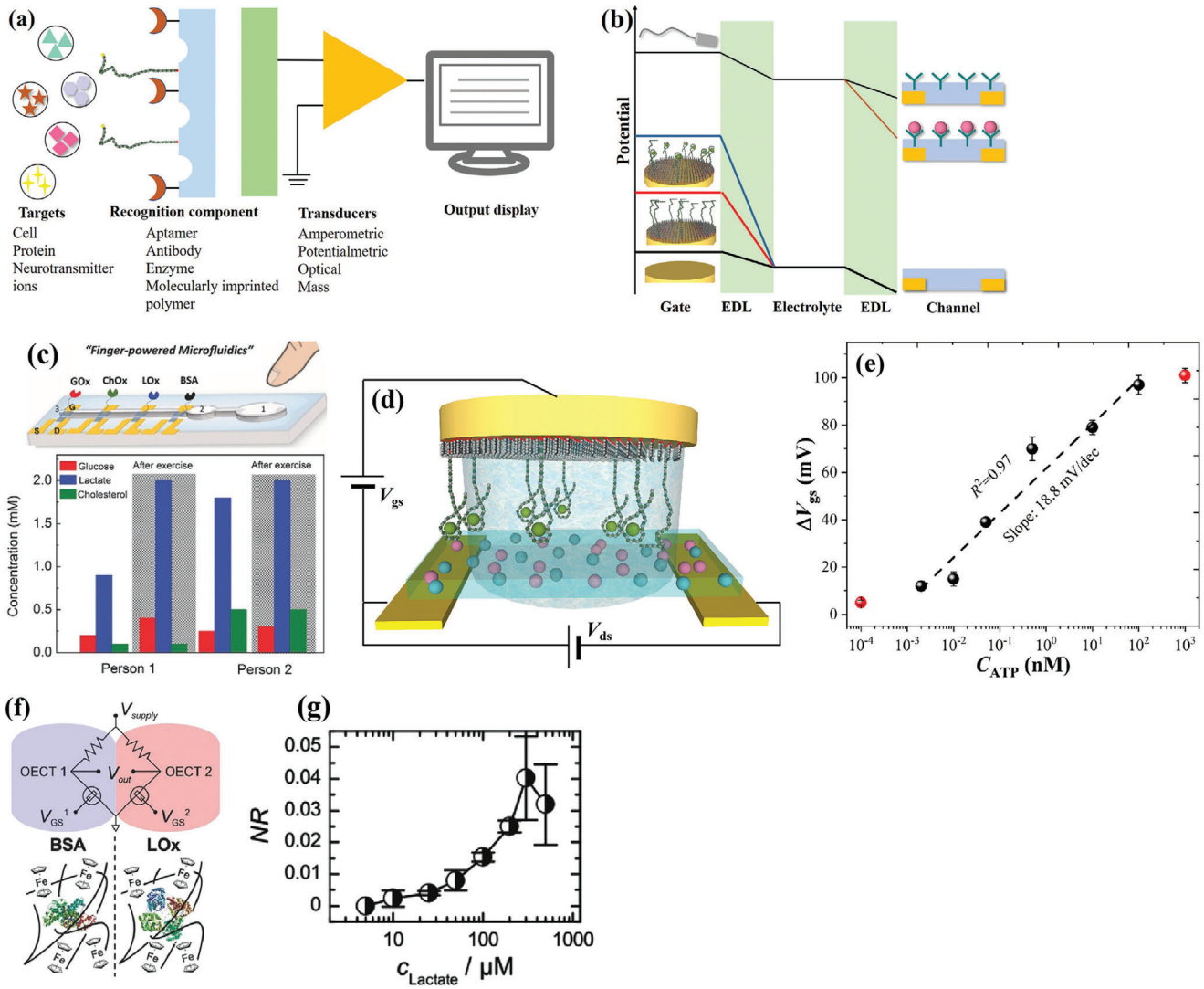

Figure 6. Different transducer principles for chemical sensing with OECTs. a) Schematic illustration of the working principle of biosensors for target detection. b) Scheme of potential drops in the Helmholtz layers: gate/electrolyte and electrolyte/channel for both channel modified and gate-modified sensors. c) Top: Scheme of the multichannel biosensor with a "finger-powered" PDMS microfluidics. Bottom: relative metabolite concentrations in saliva of different individuals before and after physical workout. Reproduced with permission.[147] Copyright 2015, Wiley-VCH GmbH. d) Scheme of an iOECT utilizing an aptamer-functionalized gate for analyte detection. e) The gate potential shift of OECTs after incubation for different concentrations of ATP. Reproduced with permission.[131] Copyright 2019, Elsevier. f) The circuit layout of a Wheatstone bridge-lactate sensor (top) and the corresponding surface modification on the two branches of the bridge (bottom). g) Calibration curve of the sensor shown in f for different lactate concentrations. Reproduced with permission.[154] Copyright 2017, Wiley-VCH GmbH.

Besides optical and magnetic detection systems, electrochemical transducers are among the most used transducer techniques. During the past two decades, several types of micro-fabricated devices have been established relying on electrochemical transduction principles such as MEAs, graphene field-effect transistors, silicon nanowire transistors, and organic electrochemical transistors. Their wide dissemination is due to their high sensitivity, versatility, small size, multichannel architecture permitting spatial resolution (chemical imaging), simultaneous multitarget detection capability, and compatibility with microelectronic systems.[137–140] The two commonly used electrochemical transducer concepts are the amperometric detection (of current) and potentiometric detection (of electrical potential), according to the registered signals generated during the specific binding or conversion event between the target molecule and the corresponding receptor.

In the following, the transduction mechanisms of OECT-based sensors are considered. Given that OECTs possess an ionic and electronic circuit, two interfacial capacitors should be taken into consideration when the organic devices are utilized as a biosensor for detecting target molecules. One is formed at the interface between the gate electrode and the electrolyte, while the second one builds up at the electrolyte/PEDOT:PSS channel interface. Both interfaces can be utilized for the attachment of receptors and the registration of binding events.[136] Correspondingly, OECTs can be operated as both potentiometric and amperometric

sensors, as illustrated in Figure 6b. In either case, the processes occurring at the receptor-modified interface cause an alteration of the effective gate voltage (V_g^{eff}) that acts on the polymer channel (Figure 6b).[141,142] V_g^{eff} can be described as: $V_g^{eff} = V_g + V_{off}$, where V_{off} is the offset voltage indicating the potential drop at the interfaces gate electrode/electrolyte and electrolyte/organic channel.[143] Thus, the shift of electrical channel characteristics (e.g., transfer characteristics) of an OECT induced by analyte binding can be attributed to the variation of the offset voltage.

In the case of a coverage-dependent modification of the capacitance of the polymer channel, a variation in the drop of gate potential occurs at the electrolyte/channel interface, while the analyte molecules are captured on the receptor film (Figure 6b). He et al. immobilized anti-*Escherichia coli* O157:H7 antibodies on PEDOT:PSS channel via a silane chemistry for the analyte detection[142] of *E. coli* O157:H7. They described the effective gate voltage via the involved interface capacitances $V_g^{eff} = \frac{C_g}{C_g + C_d} V_g$, assuming that the variations of the channel capacitance originate from the modification of the receptors during binding of the charged target analytes. The incubation of those analyte species lead to a potential shift of the transfer curve by V_g^{eff} to compensate the charges introduced by the immobilized target molecules on the polymer channel.[142]

The coverage-dependent modification of the capacitance of the gate electrode provides an alternative method to detect target molecules using PEDOT:PSS-based OECTs. Unlike the modified channel, the variation of the gate potential happens at the gate electrode/electrolyte interface, i.e., the OECT is operated as a potentiometric sensor (Figure 6b).[131,141,144] Fu et al. immobilized human epidermal growth factor receptor 2 (HER2) antibodies on the gate electrode surface, which had a high affinity to a complex of HER2/horseradish peroxidase/Au nanoparticles. The enzyme catalyzed the electrochemical conversion of H_2O_2, causing a significant variation of the gate potential and facilitated a sensitive detection of the biomarkers down to the concentration of 10^{-14} g mL^{-1}.[145] Notably, the sensitivity of OECT-based biosensor supposed to be dependent of the channel/gate area ratio. Cicoira et al. systematically investigated the influence of device geometries on their characteristics by using Pt electrodes with different areas as gate electrodes and PBS containing different H_2O_2 concentration as electrolyte. They found that devices with smaller gate/channel area ratio exhibited a lower background signal and a higher sensitivity for analytes, while this ratio had no influence on the maximum and minimum detectable analyte concentration.[146]

Pappa et al. developed a microsystem containing a pumpless finger-powered microfluidic system and an OECT-based potentiometric sensor (Figure 6c) with enzymes utilized as receptors attached to separated gate electrodes for the detection of three important biomarkers: lactate, cholesterol, and glucose.[147] Although these analytes are not specific for the nervous systems, they play a considerable role also in the metabolism of neurons.[148] In another example, Kergoat et al. added platinum nanoparticles into PEDOT:PSS for the catalytic hydrogen peroxide (H_2O_2) oxidation, proposing an enzymatic-activity-transduction OECT for the sensitive (glutamate: 4.3 A mol^{-1} L^1 cm^{-2} and acetylcholine: 4.1 A mol^{-1} L^1 cm^{-2}) and selective detection of acetylcholine (ACh) and glutamate (Glu), two crucial neurotransmitters, which show abnormal levels during Alzheimer's disease formation.[28]

Our previous work utilized OECTs as potentiometric transducer and aptamers as receptor (Figure 6d) to selectively detect adenosine triphosphate (ATP), a low weight molecules which acts as neurotransmitters in the central nervous system. The aptamer receptors where immobilized on a gold macroelectrode, which was employed as a gate electrode for the OECT. We observed a low detection limit of 10×10^{-12} M (Figure 6e), which was several orders of magnitude lower than the corresponding amperometric transducer. For the amperometric detection, the same aptamer-modified gold electrodes were used and a Faraday current originating from aptamer-associated ferrocene tags was registered. Practically, both sensors detected the same ATP/aptamer binding event; however, the amplification capabilities of the OECT enabled a strong improvement of the detection limit.[131] Another recent work utilized split aptamer sequence as dopamine receptors and OECTs as potentiometric transducers, which yielded a very low detection limit of 0.5×10^{-12} M and a high selectivity for dopamine detection.[149] It is also noteworthy, that redox-active molecules such as the catecholamine neurotransmitter (dopamine,[150] norepinephrine) can be directly detected without the need of a receptor via their amperometric conversion on either the pristine PEDOT:PSS channel or the gate electrode, see next paragraph. However, fast electrofouling and lacking of specificity is limiting the direct detection. Therefore, receptor-based sensor concepts have been established also for these molecules. Other redox and biologically-active molecules, which were successfully detected by OECT sensors are, e.g., ascorbic acid, uric acid,[126] and glucose.[147]

OECTs-based biosensors have also been utilized to measure concentration variations of physiologically-relevant ions. Romele et al. found that the ion-sensitivity of OECTs can be attributed to the ion concentration-dependent threshold voltage, which is correlated to the voltage drop at both the gate/electrolyte and the electrolyte/channel interfaces. The voltage drop at the gate/electrolyte interfaces was positively correlated with the ion concentration while the electrolyte/channel interface followed the Donnan equilibrium when the charges of PSS were completely compensated by cations from the electrolyte, thus exhibiting a cation-independent behavior at high ion concentrations.[107,151] Further work employed complementary OECTs amplifiers with different channel thickness for ion detection, which provided both ion-to-electron transconduction and signal amplification, yielding selective real-time ion (sodium) detection with a sensitivity over 2300 mV^{-1} V^{-1} dec^{-1} and a wide detection range over five orders of magnitude.[152]

Recently, further novel OECTs-based biosensor concepts emerged. Braendlein et al. combined OECTs in a Wheatstone bridge sensor circuit (Figure 6f) to detect lactate concentration of nonmalignant cells and tumor cells. This device exhibited highly sensitive metabolite detection (Figure 6g) enabled by the combination of the high amplification capability of OECTs with the inherent background subtraction capabilities (interference coming from electrolyte evaporation, electro-oxidizable compounds, etc.) of the Wheatstone bridge sensor circuit.[145] Wustoni et al. integrated an OECT channel with a nanostructured isoporous membrane, having a high affinity to amyloid-β (Aβ) oligomers, which play a crucial role in the development of Alzheimer disease. This

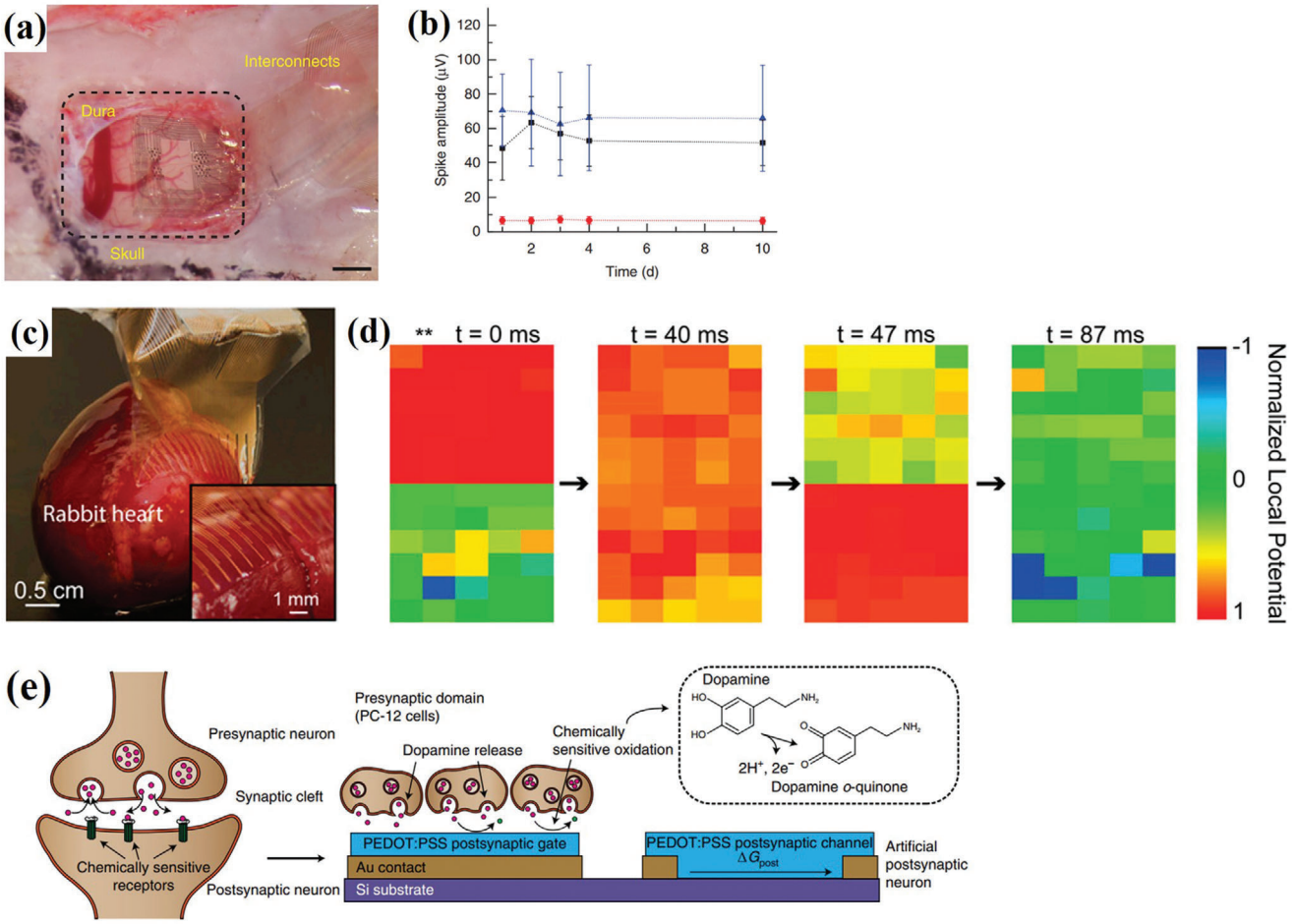

Figure 7. In vivo or in vitro applications of PEDOT:PSS-based bioelectronic devices for electrophysiological recordings. a) The NeuroGrid conforms to the surface of the rat somatosensory cortex. b) Mean and standard deviation of the amplitude of detected action potential waveforms for the rat somatosensory cortex across 10 days of recording. The average amplitude and the variability of hippocampal waveforms (blue) are larger than those of cortical waveforms (black). The red curve demonstrates the spike detection threshold. Reproduced with permission.[157] Copyright 2015, Springer Nature. c) Optical photographic image demonstrating the freestanding electrode array conforming to the surface of an ex vivo rabbit heart via surface tension. Inset shows the sensor region conforming on the surface of the heart. d) Representative normalized voltage data for 60 channels on the electrode array as their relative position to the heart. Reproduced with permission.[160] Copyright 2020, National Academy of Sciences. e) The dopamine-mediated organic neuromorphic device with postsynaptic gate electrode for dopamine oxidation and postsynaptic PEDOT:PSS-OECT channel, which is sensitive to dopamine release of PC-12 cells. Reproduced with permission.[37] Copyright 2020, Springer Nature.

novel transducer work via membrane capturing Aβ oligomers with a size larger than the pores, thus inhibiting the transport of ions into the OECT channel, resulting in a high sensitivity of 2.21×10^{-12} M for amyloid-β aggregates.[153]

3.2. In Vitro and in Vivo Probes

Monitoring signal transmission modulated by neurotransmitters and ionic fluxes could provide straightforward information about the functional connectivity-map of signaling agents and their pathological or physiological task. However, the present state-of-the-art silicon-based electrodes caused unavoidable tissue damage due to large mechanical forces, resulting in the inflammatory response when planted in the neural tissue.[155,156] As mentioned previously, in vitro or in vivo devices capable of recording electrophysiological signals over long periods have to be compliant and biocompatible to suppress those immunoreactions impairing the intimate contact to the sensor, and should facilitate an efficient signal transduction ideally by ionic-to-electronic conduction conversion. Khodagholy et al. developed a PEDOT:PSS-based neural interface array (NeuroGrid) on parylene C and recorded both local field potentials and action potentials from superficial cortical neurons (**Figure 7**a), which showed stable recordings over one week's duration (Figure 7b).[157] Their other work compared the application of PEDOT:PSS-coated electrodes with transistors for the recording of brain activity. They found that PEDOT:PSS-based transistors showed superior signal-to-noise ratio (52.7 dB) in comparison to PEDOT:PSS-coated electrode (30.2 dB) when measuring electrophysiological signals on the surface of the brain. Due to the amplification capability of the transistors,[119] they enabled the recording of

low-amplitude brain activities, which were poorly resolved with surface electrodes. Section 2.2 discussed that the channel geometry and film thickness strongly influences the signal-to-noise ratio of recorded action potentials (Figure 4h,i).[66,117] Various polymers including plastics (polyimide,[95] polycarbonate, polyethylene terephthalate,[158] parylene C[100]) and elastomers (PDMS, polyurethane etc.) have been utilized as flexible (and the latter also stretchable) substrate for bioelectronic devices.[95,158] For example, tissue penetrating probes made of OECTs embedded in parylene films (4 µm thick) could significantly alleviate the tissue damage and provided recordings with a high signal-to-noise ratio, although a rigid shuttle (SU-8, 40 µm thick) was utilized to support the probe insertion, which was delaminated from the shuttle after the precise application in the cortex.[159] Liu et al. fabricated a high-density and fully elastic electrode array (Figure 7c) by using a fluorinated elastomer as substrate comprising PEDOT:PSS coated Au electrodes to monitor the electrophysiological signals of chronic atrial fibrillation. The stretchable properties of the electrode array enabled a conformal tissue contact and better coupling with heart cells while the high electrode density facilitated high spatial resolution and investigation of cellular-level electrophysiological heterogeneity (Figure 7d).[160] In addition, to improve the versatility of PEDOT:PSS-based bioelectronics in smart and wearable electrophysiological sensors, the development of functional materials with high flexibility and durability is required to bear up scratching, wrinkling, and unexpected damage from buckling. To this end, gel-based OECTs have been developed by employing gels (e.g., gelatin[161] and poly(vinyl alcohol) (PVA)[162]) as electrolyte. Ko et al. fabricated a self-healable all-solid-state OECT by utilizing PEDOT:PSS and a nonionic surfactant Triton X-100 as the channel material and ion-conducting PVA hydrogel as the polymer electrolyte.[162] The obtained device exhibited an ultrahigh transconductance of 48 ± 5 mS, which was maintained after experiencing a cut on the channel. Lee et al. developed ultrathin flexible OECTs (2.5 µm) with nonvolatile and thin glycerol gels (6 µm), which enabled the long-term on-skin electrocardiogram (ECG) monitoring without sacrificing the signal-to-noise ratio.[100]

Recently, the in vivo recording of neurotransmitter release was reported by penetrating OECT probes with remarkable detection limits in the nM range and millisecond time range. Therefore, four transistors were fabricated on a single shank of a flexible polyethylene terephthalate substrate, which was inserted into rate brain tissue together with a second electrode used for stimulation. The catecholamine signals (mainly dopamine) were registered as direct Faraday currents at the gate electrode and amplified by the OECT transistor. The simultaneous recording of dopamine release was demonstrated at multiple striatal brain regions. With their experiments, the authors could reveal a complex cross-talk between different signaling pathways in the brain (mesolimbic and the nigrostriatal pathways).[163]

In addition, given that information processing in the brain is normally modulated by the neurotransmitters and the ionic fluxes through synapses,[164] the realization of bioinspired devices that are able to emulate the main processes of synaptic transmission and memorization have attracted intense scientific attention.[165] Gkoupidenis et al. utilized OECTs as neuromorphic devices to realize neuromorphic functions similar to the basic short-term synaptic plasticity characteristics such as short-term depression, adaptation, and dynamic filtering.[108] As mentioned above, PEDOT:PSS can also be utilized for the electrochemical detection of neurotransmitters such as catecholamines due to their redox activity.[150] Recently, Keene et al. directly couple a PEDOT:PSS-based device exhibiting neuromorphic functionality with dopaminergic cells (PC-12 cells) to realize a biohybrid synapse with synaptic plasticity mediated by neurotransmitters (Figure 7e).[37] The introduction of dopamine in the electrolyte solution caused the enhanced change of conductance due to the oxidation of dopamine at the postsynaptic gate electrode (Figure 7e). The transport of electrons from dopamine to the postsynaptic gate electrode during its oxidation was unidirectional, similar as the case of transport of neurotransmitter molecules in the synaptic cleft. Furthermore, recovery of the synaptic weight, dopamine recycling, and long-term conditioning was demonstrated, which holds the promise that PEDOT:PSS could merge artificial neuromorphic systems with networks of interconnected neurons in the future.

3.3. Neurotransmitter Pumps: Electrophoretic Migration

Besides the detection of ion and neurotransmitter signaling, their manipulation is of great interest to amplify, modulate, and inhibit electrophysiological signals in the nervous systems with the aim to regulate biological functions for fundamental studies of the brain connectivity and for disease treatment.[166] Advancements in micro- and nanotechnology as well as innovations on smart biomaterials fostered the engineer of systems that can deliver neurotransmitters, and therapeutic agents by electrical triggers with high spatiotemporal resolution ions.[167–169] Conventional technology used to regulate and stimulate biological functions (e.g., heat, muscle fatigue stimulus) usually exhibit limitations regarding the release rates (minutes to hours), restricted electronic control of the administered doses, and unsatisfying on/off ratios.[167,170,171] A concept named as "organic electronic ion pump" (OEIP) has been implemented, which can translate electric signals into electrophoretic migration of ions and neurotransmitters without necessitating liquid flow.[172–175] OEIPs connect two electrolyte reservoirs via an ion conductive (polyanion/polycations) channel. Mobile cations/anions electrostatically compensate the polymer associated bound charges while the oppositely charged mobile anions/cations are repelled.[176] A large fraction of these OEIPs are made from PEDOT:PSS due to its capability of combined electronic and ionic conduction (ion-conductive PSS phase), its large volumetric capacitance, and the processability of its associated components, which enables the fabrication of OEIP in microscale configurations.[177] In an early work, ions, e.g., K^+ were electrophoretically transported from a source medium by applying a driving voltage on the device through over-oxidized PEDOT:PSS (**Figure 8**a), which transports ions into a target medium with high temporal and spatial resolution.[174] The local boost of extracellular K^+ can depolarize the cell, thus activating the embedded Ca^{2+} pump. Ca^{2+} ions are highly important as versatile second messenger in regulating various molecular and cellular machineries, such as cell migration, fertilization, and muscle contractions.[178]

Besides transporting small ions, the OEIPs also possess great potential for precise delivery of neurotransmitters

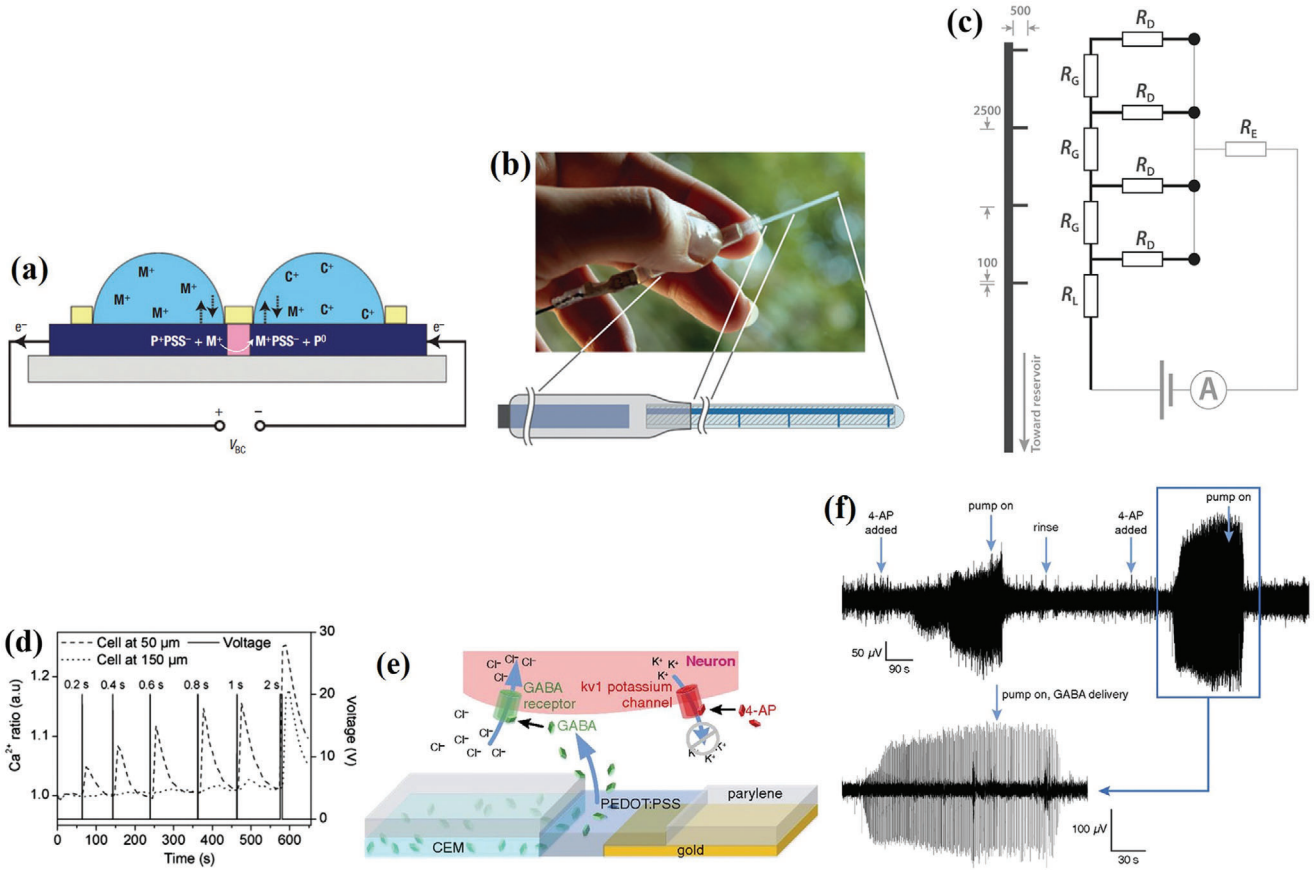

Figure 8. The organic electronic ion pump for chemical stimulation and electrical sensing: a) Schematic illustration of an OEIP. When a voltage is applied, the PEDOT on the left electrode is oxidized due to the migration of the cation M^+ to the right electrode across the over-oxidized PEDOT:PSS channel (purple), thus resulting the reduction of the PEDOT at the right side. Reproduced with permission.[174] Copyright 2007, Springer Nature. b) Image of the implantable OEIP device (top) and a schematic illustration of the components of the device: (left) electrical connection, (center) reservoir with internal electrode, and (right) delivery channel with outlets. c) The geometry of the implantable device (dimensions are given in micrometers) and the corresponding simplified electrically equivalent circuit, where R_D indicates the ionic resistance of each delivery "branch," R_E is the ionic resistance of the counter electrode and the electrolyte, respectively, and R_G represents the ionic resistance in the GABA supply channels. Reproduced with permission.[185] Copyright 2015, AAAS. d) The intracellular Ca^{2+} oscillations generated by applying a pulse-train of 20 V for different durations. Reproduced with permission.[184] Copyright 2009, Wiley-VCH GmbH. e) Pathway for diminishing 4-aminopyridine-induced epileptiform activity induced by GABA delivery. f) Mouse hippocampal epileptiform activity before and during GABA delivery recorded from the same pixel. Reproduced with permission.[186] Copyright 2016, National Academy of Sciences.

(e.g., dopamine,[179] glutamate,[180] g-aminobutyric acid (GABA),[181,182] salicylic acid,[172] and acetylcholine[183])[30,105] (Figure 8b,c). Single SH-SY5Y neuroblastoma cells were stimulated by OEIP via regulating the concentration of the neurotransmitter acetylcholine (ACh). In this study it was demonstrated that the oscillating Ca^{2+} signals in cells, which were exposed to temporally controlled release of Ach, were correlated to the distance between cells and the channel outlet (Figure 8d). Short distances could induce a rapid Ca^{2+} transient whereas the long distances resulted in unresponsive characteristics due to a significant decrease in the ACh concentration gradient. This observation points out the importance of accurate delivery of neurotransmitters to the site of treatment within the tissue, which can specify the cellular activity.[184] Jonsson et al. fabricated an implantable system that converted electric current into the delivery of the primary inhibitory neurotransmitter, GABA, in the central nervous system (Figure 8b). The four delivery points could precisely target at the spot where the injured nerve fibers joins the spinal cord (Figure 8c). This was superior to a direct injection of liquid medium carrying baclofen, a muscular relaxing drug and neurotransmitter inhibitor, or GABA to the cerebrospinal fluid. The localized delivery of the drug led to a remarkable decrease of the pain response already at low dosage without observable side effects.[185] In addition, OEIPs can be operated as multifunctional devices, capable of performing simultaneous electrical recordings of local field potentials and the delivery of neurotransmitters at the same spot and single-cell scale (Figure 8e). In this example, epileptiform activity was induced by 4-aminopyridine via GABA administration and the subsequent electrophysiological activity was recorded by PEDOT:PSS electrodes (Figure 8f).[186] The capability of OEIPs to convert electric stimuli into electrophoretic migration of neurotransmitters and ions facilitates their application in "machine-to-brain" interface devices by regulating in vivo brainstem responses.[187]

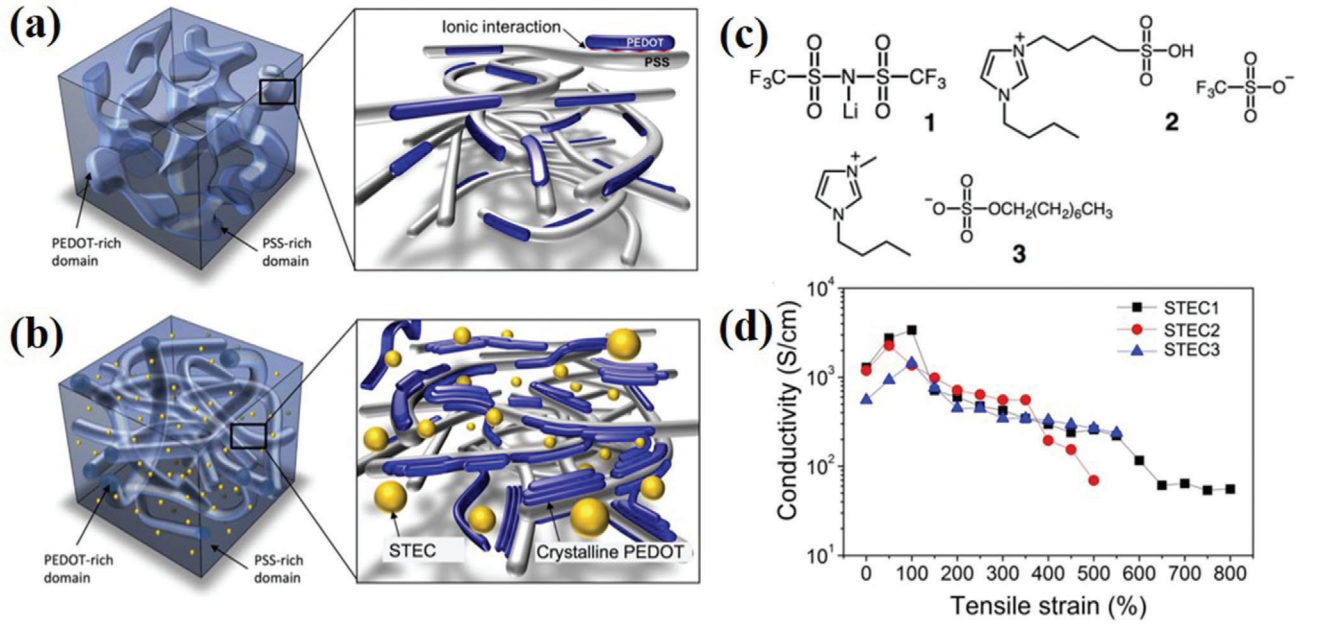

Figure 9. Highly stretchable and flexible PEDOT:PSS films: Schematic diagram representing the morphology of a) a typical PEDOT:PSS film and b) that of a stretchable PEDOT film with stretchability and electrical conductivity (STEC) enhancers. c) Chemical structure of STEC enhancers. d) Conductivity of PEDOT:PSS containing different STEC enhancers under varied strains. Reproduced with permission.[190] Copyright 2017, AAAS.

4. Recent Material Innovations: Development of PEDOT-Based Stretchable Devices and Complementary Circuits

Although PEDOT:PSS-based bioelectronics is widely used for electrophysiological recordings, as well as in wearable, flexible, and stretchable bioelectronics devices, there are still critical development steps to take to comply with the elements to cater for the complicated structures of neuronal tissue. The mechanical properties of PEDOT:PSS, whose intrinsic Young's modulus is on the order of MPa to GPa with a stretchability of not more than 10%,[98,188] were rendered toward biological applications as implants or wearable devices. Much effort was devoted to improve the stretchability of the polymer and to obtain stretchable devices, including strain engineering via forming prestrained elastomeric substrates, blending with elastomeric devices (e.g., PDMS), incorporating plasticizers (e.g., Zonyl and Triton), soft materials (e.g., poly(vinyl alcohol)), or ionic liquid. Lipomi et al. fabricated the first stretchable PEDOT:PSS-based device on prestrained PDMS substrates via blending PEDOT:PSS with DMSO and Zonyl FS-300. Wave-like buckles formed after the first stretching enabled a reversible stretchability over 1000 cycles with a strain of 10%.[189] However, the improved stretchability of PEDOT:PSS resulted in a decrease in conductivity, especially under the application of strain. The conductivity decreased from 550 S cm^{-1} at 0% strain to 13 S cm^{-1} at a strain of 188%.[189] Alternatively, the addition of ionic liquids can not only reduces the interaction between the polymer chains and thereby increase the stretchability to 50%, but also results in a strain-dependent increase of the conductivity of the polymer.[190] Wang et al. realized PEDOT:PSS films that hold both high stretchability and conductivity by blending them with different kinds of ionic liquids (**Figure 9**a–c).[190] The conductive film exhibited a conductivity over 3000 S cm^{-1} under 0% strain and over 4100 S cm^{-1} for 100% strain, the highest value reported in stretchable conductors (Figure 9d). Meanwhile, the conductivity was maintained at 3600 S cm^{-1} even after experiencing 1000 cycles of 100% strain. The significant enhancement in conductivity and stretchability of PEDOT:PSS by additives could be interpreted by i) the change of film morphology and ii) the introduction of conductivity-enhancing dopants. In addition, PEDOT:PSS can be incorporated in hydrogels,[161] for instance crosslinking the conducting polymer with an ionic liquid and subsequent polymerization of polyacrylic acid to enhance the toughness and stretchability of the hydrogel without impairing the conductivity of the polymer.[191] Murbach et al. electropolymerized EDOT in peripheral nerves directly to generate a soft, injectable conductive polymer electrode that is capable of bi-directional communication.[192] Innovations in enhancing and diversifying the mechanical and electrical properties of conducting polymer materials will foster the development of novel wearable and implantable sensor devices for neuroelectronic applications.

Another important device characteristic, which is strongly affected by the properties of the polymer material, is the transistor operation mode. Generally, transistors can be divided into two categories according to their operation mode: depletion and accumulation mode.[111] Complementary circuits that comprise both depletion- and accumulation-mode transistors could expand the sophistication level of bioelectronic devices by facilitating logical operations and eventual preprocessing of electrophysiological signals. Most of the classical PEDOT:PSS-based OECTs represent a depletion-mode operation, where the channel resistance

is small at zero gate bias. However, accumulation-mode devices are often beneficial since they possess a low power consumption and "on signals" events can be easier recorded.[193] One approach to realize accumulation mode OECTs is by blending a semiconducting polymer with PEDOT or by counter-ion exchange of the PEDOT.[124,193–195] Alternatively, novel materials were developed that are tailored toward accumulation-mode operation. Flagg et al. synthesized a new polythiophene derivative poly(3-{[2-(2-methoxyethoxy)ethoxy]methyl}thiophene-2,5-diyl) (P3MEEMT) with ethylene glycol-based side chains, which can operate OECTs in accumulation mode. This novel material exhibited faster anion injection rates than poly(3-hexylthiophene-2,5-diyl) due to the hydration of the P3MEEMT crystal lattice.[196] Nielsen et al. designed a several semiconducting polymers to explore the main structure-property guidelines essential for accumulation-mode OECTs. They found that the capacitance and the current density of thiophene copolymers (g2T-T) were significantly higher than other polymers in their work, which could be attributed to their lower ionization potentials at around 4.4 eV originating from their high degree of backbone co-planarity. The resulting properties of g2T-T-based accumulation-mode OECTs outperformed state-of-the-art PEDOT devices and demonstrated good stability in aqueous operation without the addition of crosslinkers.[197]

To date, compared with the widespread development of hole transporting semiconducting or conducting polymers for OECTs, n-type OECT channel materials are rare. This can be attributed to the limited stability of n-type polymers in aqueous media as well as irreversible oxidation and reduction within the electrochemical window imparted by the electrolyte. Recently, Giovannitti et al. prepared n-type conjugated polymers p(gNDI-gT2) and found that p(gNDI-gT2)-based OECT exhibited low transconductance (20 μS), attributing to the limiting factor of low electron mobility in this material.[120] Paterson et al. blended poly(*N*,*N*′-bis(7-glycol)-naphthalene-1,4,5,8-bis(dicarboximide)-*co*-2,2′-bithiophene-*co*-*N*,*N*′-bis(2-octyldodecyl)-naphthalene-1,4,5,8-bis(dicarboximide) (P-90) with a Lewis basic ammonium salt tetrabutylammonium fluoride (TBAF) and found that addition of 40% TBAF facilitated a well performing OECTs with a transconductance of up to 10.5 μS. More importantly, the n-type OECTs could maintain high operational stability in PBS and shelf-life.[198] First sensor application utilizing n-type OECTs transistors have been demonstrated already. Ohayon et al. employed P-90 as n-type channel material and successfully linked a redox enzyme to it to use body fluid molecules as fuel to power the device and to detect autonomously glucose.[199] These material innovations possess great potential to extend their utilization in bioelectronics and facilitate a better implantation and integration with biological systems.

5. Conclusions and Outlook

In this review, we aimed to provide an overview on the recent progress in the development of long lasting in vitro and in vivo bioelectronic devices based on PEDOT:PSS for the recording and modulation of electrophysiological as well as associated chemical signals. The main advantages of this material are its remarkable electrical property of combined ion and electron conduction, its capability of electrophoretic migration of ions and neurotransmitters, its high volumetric capacitance enabling high charge injection capability, and its compliant mechanical properties, crucial for implantable and wearable bioelectronics devices.

These features were utilized to enhance the performance of recording electrode arrays by coating them with PEDOT:PSS to reduce their impedance, to improve their charge injection capability, and to reduce eventual immune responses. Compared with conventional metallic electrodes, the presence of PEDOT:PSS improves the coupling between the electrode surface and the cellular membrane, facilitating enhanced electrical stimulation and recording of cellular signals and promotes the development of soft neuropixels. In recent years, PEDOT:PSS-based OECTs have developed to a well-established device type in the bioelectronic community. This acceptance is justified by their high transconductance values, their excellent electrochemical reversibility, their intrinsic amplification capability, and their direct ion-based communication between the channel polymer and the biological tissue, enabling high signal-to-noise ratios when recording electrophysiological and biochemical neurotransmitter signals.

The remaining challenges in this field of research permit ample room for upcoming advancements, particularly in developing long-lasting, flexible, multichannel polymer probes for simultaneous recording of electrophysiological and biochemical signals from neurons. Although the current sensors highlighted in this article have been successfully implemented for recording of extracellular potentials, the detection of subthreshold signals such as excitatory and inhibitory synaptic potentials are still lacking. Furthermore, feedback mechanisms should be established to directly study the local correlation of chemical/electrophysiological stimulation and signal recording as well as to check the specific position inside the tissue to decode synaptic activities.

Given that enzyme-based metabolite biosensing generally involves electron rather than hole-transport processes, the development of n-type organic semiconductor-based OECTs is of high interest. Considering the great amplification capabilities of OECTs, there is still plenty of room for improvement in the diversity of biosensors, since many potential receptor types have not been tested yet. Furthermore, the suitability of these sensors for chronic implantation needs to be evaluated together with the device reliability and immune responses. Additionally, integration of the recently achieved material innovations enhancing the mechanical and diversifying the electrical properties (e.g., n-type materials) of the conducting polymers needs to be implemented in future bioelectronic devices. Furthermore, integrating the bioelectronic sensors with other state-of-art components, such as supercapacitors and nanogenerators could lead to wearable or portable electronic systems for long-term and continuous monitoring of electrophysiological and biochemical signals.

Overall, remarkable advances have been made for the development of PEDOT:PSS-based bioelectronics and the obtained devices have demonstrated their capabilities in a broad variety of applications aiming on monitoring and modulating physiological and biochemical signals in various biological systems. Innovations in enhancing and diversifying the electrical and mechanical properties of the conducting polymer materials will leverage advancements in neuroscience by means of novel, flexible, long lasting in vitro and in vivo sensor devices that can communicate bidirectional with nervous tissue via combined electrophysiological and biochemical signals.

Acknowledgements

The authors acknowledge funding from the Federal Ministry of Education and Research (Germany, Grant number 031A095B). Y.L. gratefully thanks the funding from China Postdoctoral Science Foundation (Grant number 2020TQ0101) and the National Youth Foundation of China (Grant number 52003092). Furthermore, the authors are grateful to Kagithiri Srikantharajah for providing graphical support.

Open access funding enabled and organized by Projekt DEAL.

Conflict of Interest

The authors declare no conflict of interest.

Keywords

bioelectronic devices, biosensors, electrophysiological signals, ions and neurotransmitters, polymer polyethylenedioxythiophene: poly(styrene sulfonate)

Received: January 11, 2021
Revised: March 31, 2021
Published online: May 10, 2021

[1] K. Deisseroth, G. Feng, A. K. Majewska, G. Miesenböck, A. Ting, M. J. Schnitzer, *J. Neurosci.* **2006**, *26*, 10380.
[2] S. Genon, A. Reid, R. Langner, K. Amunts, S. B. Eickhoff, *Trends Cognit. Sci.* **2018**, *22*, 350.
[3] T. Someya, Z. Bao, G. G. Malliaras, *Nature* **2016**, *540*, 379.
[4] J. E. Chung, H. R. Joo, J. L. Fan, D. F. Liu, A. H. Barnett, S. Chen, C. Geaghan-Breiner, M. P. Karlsson, M. Karlsson, K. Y. Lee, *Neuron* **2019**, *101*, 21.
[5] M. L. Kringelbach, N. Jenkinson, S. L. Owen, T. Z. Aziz, *Nat. Rev. Neurosci.* **2007**, *8*, 623.
[6] C. F. Higgins, *Nature* **2007**, *446*, 749.
[7] M. E. J. Obien, K. Deligkaris, T. Bullmann, D. J. Bakkum, U. Frey, *Front. Neurosci.* **2015**, *8*, 423.
[8] G. He, N. Hu, A. M. Xu, X. Li, Y. Zhao, X. Xie, *Adv. Funct. Mater.* **2020**, *30*, 1909890.
[9] S. Kodandaramaiah, F. Flores, G. Holst, I. Wickersham, E. Brown, C. Forest, E. Boyden, *Proc. Biomed. Eng. Soc.* **2014**.
[10] K. Kitamura, B. Judkewitz, M. Kano, W. Denk, M. Häusser, *Nat. Methods* **2007**, *5*, 61.
[11] M. E. Spira, A. Hai, *Nat. Nanotechnol.* **2013**, *8*, 83.
[12] U. Frey, U. Egert, F. Heer, S. Hafizovic, A. Hierlemann, *Biosens. Bioelectron.* **2009**, *24*, 2191.
[13] L. R. Hochberg, M. D. Serruya, G. M. Friehs, J. A. Mukand, M. Saleh, A. H. Caplan, A. Branner, D. Chen, R. D. Penn, J. P. Donoghue, *Nature* **2006**, *442*, 164.
[14] A. Domínguez-Bajo, B. L. Rodilla, I. Calaresu, A. Arché-Núñez, A. González-Mayorga, D. Scaini, L. Pérez, J. Camarero, R. Miranda, E. López-Dolado, M. T. González, L. Ballerini, M. C. Serrano, *Adv. Biosyst.* **2020**, *4*, 2000117.
[15] M. C. Murphy, K. C. Chan, S.-G. Kim, A. L. Vazquez, *NeuroImage* **2020**, *169*, 352.
[16] M. Dipalo, H. Amin, L. Lovato, F. Moia, V. Caprettini, G. C. Messina, F. Tantussi, L. Berdondini, F. D. Angelis, *Nano Lett.* **2017**, *17*, 3932.
[17] J. Shi, C. Clayton, B. Tian, *Nano Res.* **2020**, *13*, 1214.
[18] C. E. Bouton, A. Shaikhouni, N. V. Annetta, M. A. Bockbrader, D. A. Friedenberg, D. M. Nielson, G. Sharma, P. B. Sederberg, B. C. Glenn, W. J. Mysiw, *Nature* **2016**, *533*, 247.
[19] R. Feiner, T. Dvir, *Nat. Rev. Mater.* **2017**, *3*, 17076.
[20] S. P. Lacour, G. Courtine, J. Guck, *Nat. Rev. Mater.* **2016**, *1*, 16063.
[21] M. Berggren, D. Nilsson, N. D. Robinson, *Nat. Mater.* **2007**, *6*, 3.
[22] F. Louwet, L. Groenendaal, J. Dhaen, J. Manca, J. Van Luppen, *Synth. Met.* **2003**, *135*, 115.
[23] F. S. Alfonso, Y. Zhou, E. Liu, A. F. McGuire, Y. Yang, H. Kantarci, D. Li, E. Copenhaver, J. B. Zuchero, H. Müller, B. Cui, *Proc. Natl. Acad. Sci. USA* **2020**, *117*, 17260.
[24] M. Ganji, E. Kaestner, J. Hermiz, N. Rogers, A. Tanaka, D. Cleary, S. H. Lee, J. Snider, M. Halgren, G. R. Cosgrove, B. S. Carter, D. Barba, I. Uguz, G. G. Malliaras, S. S. Cash, V. Gilja, E. Halgren, S. A. Dayeh, *Adv. Funct. Mater.* **2018**, *28*, 1700232.
[25] Y. Liu, J. Liu, S. Chen, T. Lei, Y. Kim, S. Niu, H. Wang, X. Wang, A. M. Foudeh, J. B.-H. Tok, Z. Bao, *Nat. Biomed. Eng.* **2019**, *3*, 58.
[26] H.-J. Kim, D. N. Heo, Y. J. Lee, S. J. Lee, J. Y. Kang, S. H. Lee, K. Kwon, S. H. Do, *Sci. Rep.* **2017**, *7*, 15245.
[27] D. Ohayon, G. Nikiforidis, A. Savva, A. Giugni, S. Wustoni, T. Palanisamy, X. Chen, I. P. Maria, E. Di Fabrizio, P. M. Costa, *Nat. Mater.* **2019**, *19*, 456.
[28] L. Kergoat, B. Piro, D. T. Simon, M. C. Pham, V. Noël, M. Berggren, *Adv. Mater.* **2014**, *26*, 5658.
[29] H. Li, H. Liu, M. Sun, Y. Huang, L. Xu, *Adv. Mater.* **2021**, *33*, 2004425.
[30] A. Williamson, J. Rivnay, L. Kergoat, A. Jonsson, S. Inal, I. Uguz, M. Ferro, A. Ivanov, T. A. Sjöström, D. T. Simon, *Adv. Mater.* **2015**, *27*, 3138.
[31] Y. Won, J. J. Lee, J. Shin, M. Lee, S. Kim, S. Gandla, *ACS Sens.* **2021**, *6*, 967.
[32] N. Cheng, L. Zhang, J. J. Kim, T. L. Andrew, *J. Mater. Chem. C* **2017**, *5*, 5787.
[33] G. D. Spyropoulos, J. N. Gelinas, D. Khodagholy, *Sci. Adv.* **2019**, *5*, eaau7378.
[34] D. S. Faber, A. E. Pereda, *Front. Mol. Neurosci.* **2018**, *11*, 427.
[35] K. Kitamura, B. Judkewitz, M. Kano, W. Denk, M. Häusser, *Nat. Methods* **2008**, *5*, 61.
[36] H. T. Shih, *Tex. Heart Inst. J.* **1994**, *21*, 30.
[37] S. T. Keene, C. Lubrano, S. Kazemzadeh, A. Melianas, Y. Tuchman, G. Polino, P. Scognamiglio, L. Cinà, A. Salleo, Y. van de Burgt, *Nat. Mater.* **2020**, *19*, 969.
[38] B. Zuber, I. Nikonenko, P. Klauser, D. Muller, J. Dubochet, *Proc. Natl. Acad. Sci. USA* **2005**, *102*, 19192.
[39] V. Lučić, T. Yang, G. Schweikert, F. Förster, W. Baumeister, *Structure* **2005**, *13*, 423.
[40] S. E. Ahmari, S. J. Smith, *Neuron* **2002**, *34*, 333.
[41] J.-M. Moon, N. Thapliyal, K. K. Hussain, R. N. Goyal, Y.-B. Shima, *Biosens. Bioelectron.* **2018**, *102*, 540.
[42] J. E. McCarthy, C. A. Hanley, L. J. Brennan, V. G. Lambertini, Y. K. Gun'ko, *J. Mater. Chem. C* **2014**, *2*, 764.
[43] D. Khodagholy, J. Rivnay, M. Sessolo, M. Gurfinkel, P. Leleux, L. H. Jimison, E. Stavrinidou, T. Herve, S. Sanaur, R. M. Owens, *Nat. Commun.* **2013**, *4*, 2133.
[44] S. Zhang, P. Kumar, A. S. Nouas, L. Fontaine, H. Tang, F. Cicoira, *APL Mater.* **2015**, *3*, 014911.
[45] B. J. Worfolk, S. C. Andrews, S. Park, J. Reinspach, N. Liu, M. F. Toney, S. C. Mannsfeld, Z. Bao, *Proc. Natl. Acad. Sci. USA* **2015**, *112*, 14138.
[46] A. M. Nardes, M. Kemerink, M. De Kok, E. Vinken, K. Maturova, R. Janssen, *Org. Electron.* **2008**, *9*, 727.
[47] J.-B. Lee, K. Rana, B. H. Seo, J. Y. Oh, U. Jeong, J.-H. Ahn, *Carbon* **2015**, *85*, 261.
[48] M. Döbbelin, R. Marcilla, M. Salsamendi, C. Pozo-Gonzalo, P. M. Carrasco, J. A. Pomposo, D. Mecerreyes, *Chem. Mater.* **2007**, *19*, 2147.
[49] Z. Yu, Y. Xia, D. Du, J. Ouyang, *ACS Appl. Mater. Interfaces* **2016**, *8*, 11629.
[50] J. Ouyang, *ACS Appl. Mater. Interfaces* **2013**, *24*, 13082.
[51] T. L. Rose, L. S. Robblee, *IEEE Trans. Biomed. Eng.* **1990**, *37*, 1118.

[52] R. A. Green, R. T. Hassarati, J. A. Goding, S. Baek, N. H. Lovell, P. J. Martens, L. A. Poole-Warren, *Macromol. Biosci.* **2012**, *12*, 494.
[53] R. T. Leung, M. N. Shivdasani, D. A. X. Nayagam, R. K. Shepherd, *IEEE Trans. Biomed. Eng.* **2014**, *62*, 849.
[54] N. Lago, K. Yoshida, K. P. Koch, X. Navarro, *IEEE. Trans. Biomed. Eng.* **2007**, *54*, 281.
[55] B. Koerbitzer, P. Krauss, C. Nick, S. Yadav, J. J. Schneider, C. Thielemann, *2D Mater.* **2016**, *3*, 024004.
[56] R. Kim, Y. Nam, *J. Neurosci. Methods* **2019**, *326*, 108369.
[57] T. J. J. Hondrich, B. Lenyk, P. Shokoohimehr, D. Kireev, V. Maybeck, D. Mayer, A. Offenhäusser, *ACS Appl. Mater. Interfaces* **2019**, *11*, 46451.
[58] Y. H. Kim, G. H. Kim, A. Y. Kim, Y. H. Han, M.-A. Chung, S.-D. Jung, *J. Neural Eng.* **2015**, *12*, 066029.
[59] Y. Lu, H. Lyu, A. G. Richardson, T. H. Lucas, D. Kuzum, *Sci. Rep.* **2016**, *6*, 33526.
[60] Y. Tao, X. Xie, W. Lv, D. M. Tang, D. Kong, Z. Huang, H. Nishihara, T. Ishii, B. Li, D. Golberg, F. Kang, T. Kyotani, Q. H. Yang, *Sci. Rep.* **2013**, *3*, 2975.
[61] D. Kireev, A. Offenhäusser, *2D Mater.* **2018**, *5*, 042004.
[62] N. V. Apollo, M. I. Maturana, W. Tong, D. A. X. Nayagam, M. N. Shivdasani, J. Foroughi, G. G. Wallace, S. Prawer, M. R. Ibbotson, D. J. Garrett, *Adv. Funct. Mater.* **2015**, *25*, 3551.
[63] F. Vitale, S. R. Summerson, B. Aazhang, C. Kemere, M. Pasquali, *ACS Nano* **2015**, *9*, 4465.
[64] S. Venkatraman, J. Hendricks, Z. A. King, A. J. Sereno, S. Richardson-Burns, D. Martin, J. M. Carmena, *IEEE Trans. Neural Syst. Rehabil. Eng.* **2011**, *19*, 307.
[65] T. D. Y. Kozai, K. Catt, Z. Du, K. Na, O. Srivannavit, R. U. M. Haque, J. Seymour, K. D. Wise, E. Yoon, X. T. Cui, *IEEE Trans. Biomed. Eng.* **2016**, *63*, 111.
[66] J. Rivnay, P. Leleux, M. Ferro, M. Sessolo, A. Williamson, D. A. Koutsouras, D. Khodagholy, M. Ramuz, X. Strakosas, R. M. Owens, *Sci. Adv.* **2015**, *1*, e1400251.
[67] A. S. Pranti, A. Schander, A. Bödecker, W. Lang, *Sens. Actuators, B* **2018**, *275*, 382.
[68] X. T. Cui, D. D. Zhou, *IEEE Trans. Neural Syst. Rehabil. Eng.* **2007**, *15*, 502.
[69] C. A. J. Thomas, P. A. Springer, G. E. Loeb, Y. Berwald-Netter, L. M. Okun, *Exp. Cell Res.* **1972**, *74*, 61.
[70] J. J. Jun, N. A. Steinmetz, J. H. Siegle, D. J. Denman, M. Bauza, B. Barbarits, A. K. Lee, C. A. Anastassiou, A. Andrei, Ç. Aydın, *Nature* **2017**, *551*, 232.
[71] E.-M. Steidl, E. Neveu, D. Bertrand, B. Buisson, *Brain Res.* **2006**, *1096*, 70.
[72] H. Yuk, B. Lu, X. Zhao, *Chem. Soc. Rev.* **2019**, *48*, 1642.
[73] D. C. Martin, G. G. Malliaras, *ChemElectroChem* **2016**, *3*, 686.
[74] M. D. Ferro, N. A. Melosh, *Adv. Funct. Mater.* **2018**, *28*, 1704335.
[75] D. R. Merrill, M. Bikson, J. G. Jefferys, *J. Neurosci. Methods* **2005**, *141*, 171.
[76] S. F. Cogan, *Annu. Rev. Biomed. Eng.* **2008**, *10*, 275.
[77] R. Huys, D. Braeken, D. Jans, A. Stassen, N. Collaert, J. Wouters, J. Loo, S. Severi, F. Vleugels, G. Callewaert, K. Verstreken, C. Bartic, W. Eberle, *Lab Chip* **2012**, *12*, 1274.
[78] J. Rivnay, H. Wang, L. Fenno, K. Deisseroth, G. G. Malliaras, *Sci. Adv.* **2017**, *3*, e1601649.
[79] X. Cui, D. C. Martin, *Sens. Actuators, B* **2003**, *89*, 92.
[80] R. Kim, Y. Nam, *J. Neurosci. Methods* **2019**, *326*, 108369.
[81] M. Sessolo, D. Khodagholy, J. Rivnay, F. Maddalena, M. Gleyzes, E. Steidl, B. Buisson, G. G. Malliaras, *Adv. Mater.* **2013**, *25*, 2135.
[82] T. Nyberg, A. Shimada, K. Torimitsu, *J. Neurosci. Methods* **2007**, *160*, 16.
[83] K. A. Ludwig, N. B. Langhals, M. D. Joseph, S. M. Richardson-Burns, J. L. Hendricks, D. R. Kipke, *J. Neural Eng.* **2011**, *8*, 014001.
[84] Y. Liu, A. F. McGuire, H.-Y. Lou, T. L. Li, J. B.-H. Tok, B. Cui, Z. Bao, *Proc. Natl. Acad. Sci. USA* **2018**, *115*, 11718.
[85] S. Zips, L. Grob, P. Rinklin, K. Terkan, N. Y. Adly, L. J. K. Weiß, D. Mayer, B. Wolfrum, *ACS Appl. Mater. Interfaces* **2019**, *11*, 32778.
[86] V. Saunier, E. Flahaut, M.-C. Blatché, C. Bergaud, A. Maziza, *Biosens. Bioelectron.* **2020**, *165*, 112413.
[87] D. N. Heo, H.-J. Kim, Y. J. Lee, M. Heo, S. J. Lee, D. Lee, S. H. Do, S. H. Lee, I. K. Kwon, *ACS Nano* **2017**, *11*, 2961.
[88] K. B. Hengen, M. E. Lambo, S. D. Van Hooser, D. B. Katz, G. G. Turrigiano, *Neuron* **2013**, *80*, 335.
[89] J.-W. Jeong, G. Shin, S. I. Park, K. J. Yu, L. Xu, J. A. Rogers, *Neuron* **2015**, *86*, 175.
[90] R. Waters, D. McNeal, W. Faloon, B. Clifford, *J. Bone Jt. Surg.* **1985**, *67*, 792.
[91] J. Bong, J. P. Ness, W. Zeng, H. Kim, J. Novello, J. Pisaniello, W. B. Lake, K. A. Ludwig, J. C. Williams, Z. Ma, *Biosens. Bioelectron.* **2019**, *142*, 111493.
[92] D. N. Heo, S.-J. Song, H.-J. Kim, Y. J. Lee, W.-K. Ko, S. J. Lee, D. Lee, S. J. Park, L. G. Zhang, J. Y. Kang, *Acta Biomater.* **2016**, *39*, 25.
[93] N. Xue, T. Sun, W. M. Tsang, I. Delgado-Martinez, S.-H. Lee, S. Sheshadri, Z. Xiang, S. Merugu, Y. Gu, S.-C. Yen, *Sens. Actuators, B* **2015**, *210*, 640.
[94] H. Yu, W. Xiong, H. Zhang, W. Wang, Z. Li, *J. Microelectromech. Syst.* **2014**, *23*, 1025.
[95] Y. Liang, M. Ernst, F. Brings, D. Kireev, V. Maybeck, A. Offenhäusser, D. Mayer, *Adv. Healthcare Mater.* **2018**, *7*, 1800304.
[96] Y. S. Zhang, A. Khademhosseini, *Science* **2017**, *356*, eaaf3627.
[97] R. Green, M. R. Abidian, *Adv. Mater.* **2015**, *27*, 7620.
[98] L. V. Kayser, D. J. Lipomi, *Adv. Mater.* **2019**, *31*, 1806133.
[99] L. Zhanshayeva, V. Favaron, G. Lubineau, *ACS Omega* **2019**, *4*, 21883.
[100] H. Lee, S. Lee, W. Lee, T. Yokota, K. Fukuda, T. Someya, *Adv. Funct. Mater.* **2019**, *29*, 1906982.
[101] F. Fu, J. Wang, H. Zeng, J. Yu, *ACS Mater. Lett.* **2020**, *2*, 1287.
[102] B. Yao, H. Wang, Q. Zhou, M. Wu, M. Zhang, C. Li, G. Shi, *Adv. Mater.* **2017**, *29*, 1700974.
[103] X. Fan, W. Nie, H. Tsai, N. Wang, H. Huang, Y. Cheng, R. Wen, L. Ma, F. Yan, Y. Xia, *Adv. Sci.* **2019**, *6*, 1900813.
[104] B. Lu, H. Yuk, S. Lin, N. Jian, K. Qu, J. Xu, X. Zhao, *Nat. Commun.* **2019**, *10*, 1043.
[105] B. W. Walker, R. P. Lara, E. Mogadam, C. H. Yu, W. Kimball, N. Annabi, *Prog. Polym. Sci.* **2019**, *92*, 135.
[106] H. S. White, G. P. Kittlesen, M. S. Wrighton, *J. Am. Chem. Soc.* **1984**, *106*, 5375.
[107] D. A. Bernards, G. G. Malliaras, *Adv. Funct. Mater.* **2007**, *17*, 3538.
[108] P. Gkoupidenis, N. Schaefer, B. Garlan, G. G. Malliaras, *Adv. Mater.* **2015**, *27*, 7176.
[109] M. Braendlein, T. Lonjaret, P. Leleux, J. M. Badier, G. G. Malliaras, *Adv. Sci.* **2017**, *4*, 1600247.
[110] M. Moser, J. F. Ponder, A. Wadsworth, A. Giovannitti, I. McCulloch, *Adv. Funct. Mater.* **2019**, *29*, 1807033.
[111] E. Zeglio, O. Inganäs, *Adv. Mater.* **2018**, *30*, 1800941.
[112] M. Sheliakina, A. Mostert, P. Meredith, *Mater. Horiz.* **2018**, *5*, 256.
[113] P. Lin, F. Yan, H. L. Chan, *ACS Appl. Mater. Interfaces* **2010**, *2*, 1637.
[114] E. Stavrinidou, P. Leleux, H. Rajaona, D. Khodagholy, J. Rivnay, M. Lindau, S. Sanaur, G. G. Malliaras, *Adv. Mater.* **2013**, *25*, 4488.
[115] J. Rivnay, P. Leleux, M. Sessolo, D. Khodagholy, T. Hervé, M. Fiocchi, G. G. Malliaras, *Adv. Mater.* **2013**, *25*, 7010.
[116] M. J. Donahue, A. Williamson, X. Strakosas, J. T. Friedlein, R. R. McLeod, H. Gleskova, G. G. Malliaras, *Adv. Mater.* **2018**, *30*, 1705031.
[117] Y. Liang, F. Brings, V. Maybeck, S. Ingebrandt, B. Wolfrum, A. Pich, A. Offenhäusser, D. Mayer, *Adv. Funct. Mater.* **2019**, *29*, 1902085.

[118] S. H. Kim, K. Hong, W. Xie, K. H. Lee, S. Zhang, T. P. Lodge, C. D. Frisbie, *Adv. Mater.* **2013**, *25*, 1822.
[119] D. Khodagholy, T. Doublet, P. Quilichini, M. Gurfinkel, P. Leleux, A. Ghestem, E. Ismailova, T. Hervé, S. Sanaur, C. Bernard, *Nat. Commun.* **2013**, *4*, 1.
[120] A. Giovannitti, C. B. Nielsen, D.-T. Sbircea, S. Inal, M. Donahue, M. R. Niazi, D. A. Hanifi, A. Amassian, G. G. Malliaras, J. Rivnay, *Nat. Commun.* **2016**, *7*, 13066.
[121] A. J. Bard, L. R. Faulkner, *Electrochemical Methods: Fundamentals and Applications*, Wiley, New York **1980**.
[122] J. Rivnay, S. Inal, A. Salleo, R. M. Owens, M. Berggren, G. G. Malliaras, *Nat. Rev. Mater.* **2018**, *3*, 1.
[123] F. Hempel, J. K. Y. Law, T. C. Nguyen, R. Lanche, A. Susloparova, X. ThangVu, S. Ingebrandt, *Biosens. Bioelectron.* **2021**, *180*, 113101.
[124] C. Cea, G. D. Spyropoulos, P. Jastrzebska-Perfect, J. J. Ferrero, J. N. Gelinas, D. Khodagholy, *Nat. Mater.* **2020**, *19*, 679.
[125] J. Viventi, D.-H. Kim, L. Vigeland, E. S. Frechette, J. A. Blanco, Y.-S. Kim, A. E. Avrin, V. R. Tiruvadi, S.-W. Hwang, A. C. Vanleer, *Nat. Neurosci.* **2011**, *14*, 1599.
[126] A. Giovannitti, D.-T. Sbircea, S. Inal, C. B. Nielsen, E. Bandiello, D. A. Hanifi, M. Sessolo, G. G. Malliaras, I. McCulloch, J. Rivnay, *Proc. Natl. Acad. Sci. USA* **2016**, *113*, 12017.
[127] S. Inal, J. Rivnay, P. Leleux, M. Ferro, M. Ramuz, J. C. Brendel, M. M. Schmidt, M. Thelakkat, G. G. Malliaras, *Adv. Mater.* **2014**, *26*, 7450.
[128] I. Uguz, M. Ganji, A. Hama, A. Tanaka, S. Inal, A. Youssef, R. M. Owens, P. P. Quilichini, A. Ghestem, C. Bernard, *Adv. Healthcare Mater.* **2016**, *5*, 3094.
[129] A. V. Marquez, G. Salinas, M. Abarkan, M. Idir, C. Brochon, G. Hadziioannou, M. Raoux, A. Kuhn, J. Lang, E. Cloutet, *Macromol. Rapid Commun.* **2020**, *41*, 2000134.
[130] Y. Y. Broza, X. Zhou, M. Yuan, D. Qu, Y. Zheng, R. Vishinkin, M. Khatib, W. Wu, H. Haick, *Chem. Rev.* **2019**, *119*, 11761.
[131] Y. Liang, C. Wu, G. Figueroa-Miranda, A. Offenhäusser, D. Mayer, *Biosens. Bioelectron.* **2019**, *144*, 111668.
[132] S. Kumar, P. Rai, J. G. Sharma, A. Sharma, B. D. Malhotra, *Adv. Mater. Technol.* **2016**, *1*, 1600056.
[133] S. S. Gul, K. W. Huesgen, K. K. Wang, K. Mark, J. A. Tyndall, *Med. Hypotheses* **2017**, *105*, 34.
[134] A. Lleó, R. Núñez-Llaves, D. Alcolea, C. Chiva, D. Balateu-Paños, M. Colom-Cadena, G. Gomez-Giro, L. Muñoz, M. Querol-Vilaseca, J. Pegueroles, L. Rami, A. Lladó, J. L. Molinuevo, M. Tainta, J. Clarimón, T. Spires-Jones, R. Blesa, J. Fortea, P. Martínez-Lage, R. Sánchez-Valle, E. Sabidó, À. Bayés, O. Belbin, *Mol. Cell. Proteomics* **2019**, *18*, 546.
[135] P. C. Guest, *Reviews on Biomarker Studies in Psychiatric and Neurodegenerative Disorders*, Springer, Berlin **2019**, 1118.
[136] R. A. Picca, K. Manoli, E. Macchia, L. Sarcina, C. D. Franco, N. Cioffi, D. Blasi, R. Österbacka, F. Torricelli, G. Scamarcio, L. Torsi, *Adv. Funct. Mater.* **2019**, *30*, 1904513.
[137] R. C. Hughes, A. J. Ricco, M. A. Butler, S. J. Martin1, *Science* **1991**, *254*, 74.
[138] J. Janata, *Proc. IEEE* **2003**, *91*, 864.
[139] B. J. Privett, J. H. Shin, M. H. Schoenfisch, E. Sensors, *Anal. Chem.* **2008**, *80*, 4499.
[140] J. Marzioch, J. Kieninger, A. Weltin, H. Flamm, K. Aravindalochanan, J. A. Sandvik, E. O. Pettersen, Q. Peng, G. A. Urban, *Lab Chip* **2018**, *18*, 3353.
[141] D. A. Bernards, D. J. Macaya, M. Nikolou, J. A. DeFranco, S. Takamatsu, G. G. Malliaras, *J. Mater. Chem.* **2008**, *18*, 116.
[142] R.-X. He, M. Zhang, F. Tan, P. H. Leung, X.-Z. Zhao, H. L. Chan, M. Yang, F. Yan, *J. Mater. Chem.* **2012**, *22*, 22072.
[143] P. Lin, X. Luo, I. M. Hsing, F. Yan, *Adv. Mater.* **2011**, *23*, 4035.
[144] H. Tang, F. Yan, P. Lin, J. Xu, H. L. Chan, *Adv. Funct. Mater.* **2011**, *21*, 2264.
[145] Y. Fu, N. Wang, A. Yang, H. K. w. Law, L. Li, F. Yan, *Adv. Mater.* **2017**, *29*, 1703787.
[146] F. Cicoira, M. Sessolo, O. Yaghmazadeh, J. A. DeFranco, S. Y. Yang, G. G. Malliaras, *Adv. Mater.* **2010**, *22*, 1012.
[147] A. M. Pappa, V. F. Curto, M. Braendlein, X. Strakosas, M. J. Donahue, M. Fiocchi, G. G. Malliaras, R. M. Owens, *Adv. Healthcare Mater.* **2016**, *5*, 2295.
[148] R. Sangubotla, J. Kim, *TrAC, Trends Anal. Chem.* **2018**, *105*, 240.
[149] Y. Liang, T. Guo, L. Zhou, A. Offenhäusser, D. Mayer, *Materials* **2020**, *13*, 2577.
[150] I. Gualandi, D. Tonelli, F. Mariani, E. Scavetta, M. Marzocchi, B. Fraboni, *Sci. Rep.* **2016**, *6*, 35419.
[151] P. Romele, M. Ghittorelli, Z. M. Kovács-Vajna, F. Torricelli, *Nat. Commun.* **2019**, *10*, 3044.
[152] P. Romele, P. Gkoupidenis, D. A. Koutsouras, K. Lieberth, Z. M. Kovács-Vajna, P. W. Blom, F. Torricelli, *Nat. Commun.* **2020**, *11*, 3743.
[153] S. Wustoni, S. Wang, J. R. Alvarez, T. C. Hidalgo, S. P. Nunes, S. Inal, *Biosens. Bioelectron.* **2019**, *143*, 111561.
[154] M. Braendlein, A.-M. Pappa, M. Ferro, A. Lopresti, C. Acquaviva, E. Mamessier, G. G. Malliaras, R. M. Owens, *Adv. Mater.* **2017**, *29*, 1605744.
[155] K. Woeppel, Q. Yang, X. T. Cu, *Curr. Opin. Biomed. Eng.* **2017**, *4*, 21.
[156] J. A. Fairfield, *Adv. Funct. Mater.* **2018**, *28*, 1701145.
[157] D. Khodagholy, J. N. Gelinas, T. Thesen, W. Doyle, O. Devinsky, G. G. Malliaras, G. Buzsáki, *Nat. Neurosci.* **2015**, *18*, 310.
[158] C. Yao, Q. Li, J. Guo, F. Yan, I. M. Hsing, *Adv. Healthcare Mater.* **2015**, *4*, 528.
[159] A. Williamson, M. Ferro, P. Leleux, E. Ismailova, A. Kaszas, T. Doublet, P. Quilichini, J. Rivnay, B. Rózsa, G. Katona, *Adv. Mater.* **2015**, *27*, 4405.
[160] J. Liu, X. Zhang, Y. Liu, M. Rodrigo, P. D. Loftus, J. Aparicio-Valenzuela, J. Zheng, T. Pong, K. J. Cyr, M. Babakhanian, *Proc. Natl. Acad. Sci. USA* **2020**, *117*, 14769.
[161] Y. J. Jo, K. Y. Kwon, Z. U. Khan, X. Crispin, T.-i. Kim, *ACS Appl. Mater. Interfaces* **2018**, *10*, 39083.
[162] J. Ko, X. Wu, A. Surendran, B. T. Muhammad, W. L. Leong, *ACS Appl. Mater. Interfaces* **2020**, *12*, 33979.
[163] K. Xie, N. Wang, X. Lin, Z. Wang, X. Zhao, P. Fang, H. Yue, J. Kim, J. Luo, S. Cui, F. Yan, P. Shi, *Elife* **2020**, *9*, e50345.
[164] L. Abbott, W. G. Regehr, *Nature* **2004**, *431*, 796.
[165] D. Kuzum, S. Yu, H. P. Wong, *Nanotechnology* **2013**, *24*, 382001.
[166] F. Pei, B. Tian, *Adv. Funct. Mater.* **2020**, *30*, 1906210.
[167] N. A. Peppas, D. S. Van Blarcom, *J. Controlled Release* **2016**, *240*, 142.
[168] W. Gu, X. Zhu, N. Futai, B. S. Cho, S. Takayama, *Proc. Natl. Acad. Sci. USA* **2004**, *101*, 15861.
[169] D. Olvera, M. G. Monaghan, *Adv. Drug Delivery Rev.* **2020**, *170*, 396.
[170] P. M. George, D. A. LaVan, J. A. Burdick, C. Y. Chen, E. Liang, R. Langer, *Adv. Mater.* **2006**, *18*, 577.
[171] H. R. Culver, J. R. Clegg, N. A. Peppas, *Acc. Chem. Res.* **2017**, *50*, 170.
[172] M. Seitanidou, R. Blomgran, G. Pushpamithran, M. Berggren, D. T. Simon, *Adv. Healthcare Mater.* **2019**, *8*, 1900813.
[173] T. A. Sjöström, M. Berggren, E. O. Gabrielsson, P. Janson, D. J. Poxson, M. Seitanidou, D. T. Simon, *Adv. Mater. Technol.* **2018**, *3*, 1700360.
[174] J. Isaksson, P. Kjäll, D. Nilsson, N. Robinson, M. Berggren, A. Richter-Dahlfors, *Nat. Mater.* **2007**, *6*, 673.
[175] I. Bernacka-Wojcik, M. Huerta, K. Tybrandt, M. Karady, M. Y. Mulla, D. J. Poxson, E. O. Gabrielsson, K. Ljung, D. T. Simon, M. Berggren, E. Stavrinidou, *Small* **2019**, *15*, 1902189.
[176] D. T. Simon, E. O. Gabrielsson, K. Tybrandt, M. Berggren, *Chem. Rev.* **2016**, *116*, 13009.
[177] D. Ohayon, S. Inal, *Adv. Mater.* **2020**, *32*, 2001439.

[178] M. J. Berridge, M. D. Bootman, H. L. Roderick, *Nat. Rev. Mol. Cell Biol.* **2003**, *4*, 517.
[179] C. M. Proctor, C. Y. Chan, L. Porcarelli, E. Udabe, A. Sanchez-Sanchez, I. d. Agua, D. Mecerreyes, G. G. Malliaras, *Chem. Mater.* **2019**, *31*, 7080.
[180] D. T. Simon, S. Kurup, K. C. Larsson, R. Hori, K. Tybrandt, M. Goiny, E. W. H. Jager, M. Berggren, B. Canlon, A. Richter-Dahlfors, *Nat. Mater.* **2009**, *8*, 742.
[181] I. Uguz, C. M. Proctor, V. F. Curto, A. M. Pappa, M. J. Donahue, M. Ferro, R. M. Owens, D. Khodagholy, S. Inal, G. G. Malliaras, *Adv. Mater.* **2017**, *29*, 1701217.
[182] C. M. Proctor, A. Slézia, A. Kaszas, A. Ghestem, I. d. Agua, A.-M. Pappa, C. Bernard, A. Williamson, G. G. Malliaras, *Sci. Adv.* **2018**, *4*, eaau1291.
[183] C. M. Proctor, I. Uguz, A. Slezia, V. Curto, S. Inal, A. Williamson, G. G. Malliaras, *Adv. Biosyst.* **2019**, *3*, 1800270.
[184] K. Tybrandt, K. C. Larsson, S. Kurup, D. T. Simon, P. Kjäll, J. Isaksson, M. Sandberg, E. W. Jager, A. Richter-Dahlfors, M. Berggren, *Adv. Mater.* **2009**, *21*, 4442.
[185] A. Jonsson, Z. Song, D. Nilsson, B. A. Meyerson, D. T. Simon, B. Linderoth, M. Berggren, *Sci. Adv.* **2015**, *1*, e1500039.
[186] A. Jonsson, S. Inal, I. Uguz, A. J. Williamson, L. Kergoat, J. Rivnay, D. Khodagholy, M. Berggren, C. Bernard, G. G. Malliaras, *Proc. Natl. Acad. Sci. USA* **2016**, *113*, 9440.
[187] K. C. Larsson, P. Kjäll, A. Richter-Dahlfors, *Biochim. Biophys. Acta, Gen. Subj.* **2013**, *1830*, 4334.
[188] D. Gao, K. Parida, P. S. Lee, *Adv. Funct. Mater.* **2020**, *30*, 1907184.
[189] D. J. Lipomi, J. A. Lee, M. Vosgueritchian, B. C.-K. Tee, J. A. Bolander, Z. Bao, *Chem. Mater.* **2012**, *24*, 373.
[190] Y. Wang, C. Zhu, R. Pfattner, H. Yan, L. Jin, S. Chen, F. Molina-Lopez, F. Lissel, J. Liu, N. I. Rabiah, Z. Chen, J. W. Chung, C. Linder, M. F. Toney, B. Murmann, Z. Bao, *Sci. Adv.* **2017**, *3*, e1602076.
[191] V. R. Feig, H. Tran, M. Lee, Z. Bao, *Nat. Commun.* **2017**, *9*, 2740.
[192] J. M. Murbach, S. Currlin, A. Widener, Y. Tong, S. Chhatre, V. Subramanian, D. C. Martin, B. N. Johnson, K. J. Otto, *MRS. Commun.* **2018**, *8*, 1043.
[193] E. Zeglio, M. M. Schmidt, M. Thelakkat, R. Gabrielsson, N. Solin, O. Inganäs, *Chem. Mater.* **2017**, *29*, 4293.
[194] E. Zeglio, M. Vagin, C. Musumeci, F. N. Ajjan, R. Gabrielsson, X. T. Trinh, N. T. Son, A. Maziz, N. Solin, O. Inganäs, *Chem. Mater.* **2015**, *27*, 6385.
[195] E. Zeglio, J. Eriksson, R. Gabrielsson, N. Solin, O. Inganäs, *Adv. Mater.* **2017**, *29*, 1605787.
[196] L. Q. Flagg, C. G. Bischak, J. W. Onorato, R. B. Rashid, C. K. Luscombe, D. S. Ginger, *J. Am. Chem. Soc.* **2019**, *141*, 4345.
[197] C. B. Nielsen, A. Giovannitti, D.-T. Sbircea, E. Bandiello, M. R. Niazi, D. A. Hanifi, M. Sessolo, A. Amassian, G. G. Malliaras, J. Rivnay, *J. Am. Chem. Soc.* **2016**, *138*, 10252.
[198] A. F. Paterson, A. Savva, S. Wustoni, L. Tsetseris, B. D. Paulsen, H. Faber, A. H. Emwas, X. Chen, G. Nikiforidis, T. C. Hidalgo, *Nat. Commun.* **2020**, *11*, 1.
[199] D. Ohayon, G. Nikiforidis, A. Savva, A. Giugni, S. Wustoni, T. Palanisamy, X. Chen, I. P. Maria, E. D. Fabrizio, P. M. F. J. Costa, I. McCulloch, S. Inal, *Nat. Mater.* **2020**, *19*, 456.

Yuanying Liang received her B.S. degree and M.S. degree in polymer processing and engineering from Sichuan University, China, in 2012 and 2015, respectively. She gained her Ph.D. degree in chemistry from the RWTH Aachen University, Germany, in 2019 under the supervision of Prof. Andreas Offenhäusser and Dr. Dirk Mayer. She is currently working as a postdoc in Luminescent Material and Devices National Key Laboratory in South China University of Technology, China. Her main research interests are in the field of organic bioelectronic devices and polymer physics.

Andreas Offenhäusser did his doctoral studies at the University of Ulm, Germany, and received his Dr. rer. nat. degree in 1989. After two years working in industry, he joined the Frontier Research Program, RIKEN, Japan as Postdoctoral Researcher and in 1994 the Max Planck Institute or Polymer Research in Mainz, Germany. In 2001 he received venia legendi from the Faculty of Science, Eberhard Karls University, Tübingen, Germany and was appointed as director of the bioelectronic department at the Institute of Biological Information Processing, Forschungszentrum Jülich. Since 2002 he is full professor of experimental physics at RWTH Aachen University.

Sven Ingebrandt did his doctoral studies at the Max-Planck-Institute for Polymer Research, Mainz, Germany, and received his Dr. rer. nat. degree (2001) from the Johannes-Gutenberg-University Mainz, Germany. After one year as a postdoctoral researcher at the Frontier Research Program, RIKEN, Japan, he joined, in 2002, the Institute of Bio- and Nanosystems at the Forschungszentrum Jülich, Germany. From 2008 to 2017, he was professor of biomedical instrumentation at the University of Applied Sciences Kaiserslautern, Germany. In 2018, he moved to the RWTH Aachen University onto a chair professorship for Micro- and Nanosystems and he is director of the Institute of Materials in Electrical Engineering 1.

Dirk Mayer did his doctoral studies in chemistry at the University of Leipzig, Germany, and received his Dr. rer. nat. degree in 1999. After two year as a postdoctoral researcher at the Institute of Interface Science and Vacuum Physics, Forschungszentrum Jülich, Germany, he joined the Institute of Biological Information Processing, Bioelectronics IBI-3, Forschungszentrum Jülich, Germany, as principle investigator in 2002. His main research areas are the development of nanoscale bio-inorganic hybrid systems and of biosensors.